Fuel Processing Technology 286 (2026) 108449

Contents lists available at ScienceDirect

Fuel Processing Technology

journal homepage: www.elsevier.com/locate/fuproc

New integrated CCS and CCU schemes with small-scale biogas-fired combined-cycle power plant: A Comparative techno-economic assessment

Mostafa Jafari [a], Kamran Ghasemzadeh [b,*], Maria-Chiara Ferrari [b], Adele Brunetti [c,*], Simona Liguori [d], Rashid Jamshidi [e]

[a] School of Chemical Engineering, College of Engineering, University of Tehran, Tehran, Iran
[b] School of Engineering, University of Edinburgh, UK
[c] Institute on Membrane Technology of the National Research Council (CNR-ITM), via P. Bucci 17C, Rende (CS), 87036, Italy
[d] Department of Chemical and Biomolecular Engineering, Clarkson University, USA
[e] Department of Engineering, Manchester Metropolitan University, Manchester M1 5GD, UK

ARTICLE INFO

Keywords:
Carbon capture and storage (CCS)
Carbon capture and utilization (CCU)
Biogas-fired combined-cycle power plant (CCPP)
Membrane / Membrane reactor
Techno-economic assessment
Net-Zero Approach

ABSTRACT

This study presents a unified techno-economic assessment of conventional and membrane-enabled carbon capture and storage (CCS) and carbon capture and utilization (CCU) integrated into small-scale biogas-fired combined-cycle power plants. A novel contribution is the first side-by-side evaluation of a fully membrane-based post-combustion CO_2 capture system for CCS and a membrane reactor-assisted CCU configuration within a consistent Aspen HYSYS framework under identical system boundaries. Membrane integration significantly enhanced energy performance, eliminating hot-utility demand and reducing specific energy consumption by 43% in CCS. In CCU, the membrane reactor achieved higher hydrocarbon selectivity at residence times 62% shorter than in conventional reactors, implying proportional reductions in reactor size and capital expenditure. Capital costs decreased by 12% for CCS and up to 24% for CCU. Despite higher utility demand, membrane-assisted CCU increased value-added fuel production by 31.3%. Sensitivity analysis identified membrane cost, lifetime, and utility prices as key levelised cost of electricity (LCOE) drivers. A 300% increase in natural gas prices raised LCOE from −96 to 584 USD/MWh, while hydrogen prices above 3000 USD/t rendered several CCU pathways unviable. Overall, membrane-enabled systems show strong potential, contingent on optimised membrane performance and hydrogen costs.

1. Introduction

In the face of escalating climate change, reducing greenhouse gas (GHG) emissions, particularly carbon dioxide (CO_2), has become a global imperative [1]. As the most prevalent anthropogenic GHG, CO_2 significantly contributes to global warming due to its long atmospheric lifetime and cumulative impact. The energy sector, especially fossil-fuel-based power generation, accounts for a substantial portion of global CO_2 emissions, making it a primary focus for defossilization strategies and technological innovations [2]. Carbon capture and storage (CCS) and Carbon capture utilization (CCU) offer promising pathways to manage emissions from industrial and energy systems [3,4]. CCS captures CO_2 for secure storage in geological formations, such as saline aquifers or depleted oil reservoirs [5]. Conversely, CCU converts captured CO_2 into marketable products, including synthetic fuels, chemicals, and construction materials. Despite their potential, both technologies face challenges in energy efficiency, process integration, and scalability [6].

Carbon capture can be achieved through different technological routes, including chemical absorption, physical adsorption, cryogenic separation, and membrane-based processes. Carbon molecular sieve (CMS) membranes combine high CO_2 permeability and selectivity with excellent thermal and chemical stability, enabling durable operation under harsh conditions. Their resistance to plasticization and proven techno-economic benefits highlight them as an efficient and competitive alternative to conventional amine-based capture technologies [7–10]. Combined-cycle power plants (CCPPs) are among the most efficient configurations for electricity generation [11]. When fueled by biogas, a renewable energy source derived from the anaerobic fermentation of organic waste, they offer a low-carbon alternative to conventional fossil-based power generation. Biogas-fueled CCPPs not only reduce dependence on fossil fuels but also contribute to sustainable energy transitions

* Corresponding authors.
E-mail addresses: kghasemz@ed.ac.uk (K. Ghasemzadeh), a.brunetti@itm.cnr.it (A. Brunetti).

https://doi.org/10.1016/j.fuproc.2026.108449
Received 4 March 2026; Received in revised form 1 April 2026; Accepted 2 April 2026
Available online 6 April 2026

Nomenclature

AC	Air Cooler
ASPEN	Advanced System for Process Engineering
BGD	BioGas Demand
BLI	Battery Limits Investment
CAPEX	Capital Expenditure
CCGT	Combined Cycle Gas Turbines
CCPP	Combined-Cycle Power Plants
CCS	Carbon Capture and Storage
C-CCS	Conventional Carbon Capture and Storage
CCU	Carbon Capture and Utilization
C-CCU	Conventional Carbon Capture and Utilization
CE	Chemical Efficiency
CEPCI	Chemical Engineering Plant Cost Index
CHP	Combined Heat and Power
CMS	Carbon Molecular Sieve
COVID	Coronavirus Disease
CWD	Cooling Water Demand
FFD	Furnace Fuel Demand
FO	Fuel Output
GCO_2	Generated CO_2
GHG	Greenhouse Gas
GPU	Gas Permeance Unit
HHV	Higher Heating Value
HPSD	High-Pressure Steam Demand
HRSG	Heat Recovery Steam Generator
ICO	Indirect CO_2 Output
IHS	Information Handling Services
IRR	Internal Rate of Return
KPI	Key Performance Indicators
LCNC	Levelized Cost of Net Carbon
LCOE	Levelized Costs of Electricity
LPSD	Low Pressure Steam Demand
MB-CCS	Membrane Based Carbon Capture and Storage
MB-CCU	Membrane Based Carbon Capture and Utilization
MEA	Monoethanolamine
MMBTU	Million British Thermal Units
MMSCFD	Million standard cubic feet
MR	Membrane Reactor
MU	Make Up
MUA	Make Up Amine
MUSD	Million United States dollar
MUW	Make Up Water
MW	Megawatt
MWh	Megawatt-hour
NO	N_2 Output
NPV	Net Present Value
OPEX	Operating expenditure
PBP	Payback Period
PFD	Process Flow Diagram
PSA	Pressure Swing Adsorption
PR	Peng–Robinson
RD	Refrigerant Demand
ROR	Rate of Return
SRT	Specific Residence Time
TCI	Total Capital Investment
TEC	Total Equipment Cost
TED	Total Energy Demand
TFC	Total Fixed Capital
TIC	Total Installed Cost
TRL	Technology Readiness Levels
TWC	Total Working Capital
USD	United States dollar
WO	Wastewater Output
WW	Wastewater

Symbols

E	kJ/kg mol, Activation energy for a chemical reaction
C_e	(m$), Cost of equipment (million USD)
$\dot{m}_{fuel}$	kg/h, Mass flow rate of synthesized fuel
$\dot{m}_{BG}$	kg/h, Mass flow rate of biogas feed
LHV_{Lfuel}	kJ/kg, Lower heating value of the liquid fuel product
LHV_{BG}	kJ/kg, Lower heating value of the biogas
P_{net}	kW, Net electrical power output exported to the grid
Q_{CW}	kW, Cooling water energy consumption
Q_{LPS}	kW, Low-pressure steam energy consumption
Q_{HPS}	kW, High-pressure steam energy consumption
Q_{FF}	kW, Auxiliary furnace fuel energy consumption
Q_{REF}	kW, Refrigerant energy consumption
Q_{Total}	kW, Total utility energy consumption
$\dot{m}_{generated\ CO2}$	kg/h, Mass flow rate of direct CO_2 emissions
$\dot{m}_{N2}$	kg/h, Mass flow rate of nitrogen discharged
$\dot{m}_{waste\ water}$	kg/h, Mass flow rate of generated wastewater
τ	min, Residence Time
J_i	m^3/h, Volumetric permeation flux of component i through the membrane
A	m^2, Effective membrane area
k_{ei}	m^3/m^2.s.bar, Permeance coefficient of component *i*
$P_{i,retentate}$	bar, Partial pressure of component i on the retentate side
$P_{i,permeate}$	bar, Partial pressure of component i on the permeate side

and decentralised energy systems [12].

Integrating CCS or CCU with biogas-fired CCPPs can further enhance their environmental performance by mitigating or valorizing CO_2 emissions, aligning with net-zero energy goals. Recent studies have explored CCS and CCU integration in both fossil-fueled and renewable-based energy systems. Van der Spek et al. [13] conducted a comparative techno-economic study of membrane-based and monoethanolamine (MEA)-based post-combustion carbon dioxide capture systems integrated into combined cycle gas turbines (CCGTs) operating under part-load conditions. Their analysis showed that, while MEA systems demonstrated higher capture efficiency and lower energy penalties, membrane-based systems offered cost reduction potential at low carbon dioxide recovery levels. However, membrane configurations resulted in higher levelized electricity costs, ranging from 80 to 95 USD/MWh, depending on membrane performance and operating mode. Asadi and Kazempoor [14] investigated the performance of flexible membrane-based post-combustion CO_2 capture systems across varying operating conditions. Their findings highlighted that counter-current membrane configurations with sweep gas could achieve capture costs as low as 22.76 USD/t CO_2, emphasizing the role of high-permeability membranes and energy-efficient compression schemes in minimizing costs. More recently, Akrami et al. [15] proposed a biogas-fueled combined heat and power (CHP) system integrated with an MEA-based CCU unit designed for greenhouse CO_2 utilization. Their thermodynamic and economic analysis reported a CO_2 capture efficiency of 96.1%, a payback period of 4.8 years, and an LCOE of 46.16 USD/MWh, demonstrating the viability of small-scale bio-CCU systems for distributed energy and carbon valorization. Biogas from organic waste enables

a sustainable, low-carbon option for power generation. Integrating CCS or CCU technologies further improves their environmental performance by enabling CO_2 mitigation or valorization.

However, most of the aforementioned studies focus primarily on either specific capture routes or particular process scales, without providing a consistent comparison of CCS and CCU pathways under unified operating assumptions. While these studies successfully demonstrated the feasibility and advantages of different membrane or amine approaches, they often neglect cross-system interactions and the economic trade-offs between storage and utilization options. This limits their applicability to decision-making for actual carbon management implementations. Although extensive research [16,17] has investigated CCS and CCU technologies, a comprehensive system-level evaluation of their cost competitiveness in small-scale biogas-fired combined-cycle power plants (CCPPs) remains limited, particularly for membrane-integrated configurations. Most existing studies focus on fossil-fuel-based systems, small CHP units [18,19], or isolated capture processes, without considering the integrated interactions between power generation, CO_2 separation, hydrogen management, and downstream utilization. These omissions highlight the need for a more holistic and critically balanced evaluation of the techno-economic performance of CCS and CCU strategies in renewable-based systems. In addition, the economic robustness of membrane-based CCS and CCU pathways under the volatile post-COVID energy and hydrogen markets has not been systematically assessed.

It should also be noted that the availability of biogas inherently limits plant capacity, and small-scale CCPPs (below 20 MW) generally exhibit moderate internal rates of return due to scale-related capital intensity. Consequently, the objective of this work is not to demonstrate high absolute profitability, but to provide a consistent techno-economic comparison of alternative carbon management strategies under identical feedstock and operating conditions.

To address these gaps, this study develops a unified Aspen HYSYS–based process simulation combined with inflation-adjusted techno-economic modeling of membrane-integrated CCS and CCU configurations, benchmarked against conventional reference systems across four scenarios. Within a consistent modeling framework and identical system boundaries, CCS and CCU pathways are evaluated side by side to enable direct comparison of energy penalties, variations in net power output, capital investment requirements, and overall economic performance. A key contribution of this work is the systematic assessment of two membrane-enabled configurations within the same CCPP framework: (i) a pure membrane-based CO_2 capture unit for CCS and (ii) a membrane reactor–assisted CCU pathway that couples CO_2 conversion with selective hydrogen recovery. Unlike conventional post-combustion capture systems, the proposed CCS configuration relies entirely on membrane separation, while the CCU pathway employs membrane reactor technology as a process-intensification strategy.

2. Methodology

2.1. Process design

This study employs Aspen HYSYS v14.1 to simulate a biogas-fired combined-cycle power plant (CCPP) integrated with CO_2 capture and either storage (CCS) or utilization (CCU), as depicted in Fig. S1. Four configurations are evaluated to assess technical and economic performance comprehensively:

- Conventional CCS (C-CCS)
- Membrane-based CCS (MB-CCS)
- Conventional CCU (C-CCU)
- Membrane-based CCU (MB-CCU)

All simulations use a fixed biogas feed composition and flow rate, with the Peng–Robinson (PR) equation of state to model thermodynamic behavior. Conventional configurations employ the Acid Gas–Chemical Solvent fluid package [20–22], for biogas sweetening due to its accuracy for amine-based CO_2 absorption, while membrane-based sweetening and other process units use the PR fluid package for consistency [23,24].

2.2. Model development for CCS integration

2.2.1. Conventional CCS units integrated with biogas fired power plant (C-CCS)

Fig. S2 presents the process flow diagram (PFD) of the C-CCS configuration used for both simulation and economic evaluation. This configuration comprises:

- Amine-based biogas upgrading unit
- Combined-cycle power generation (CCPP) unit
- Amine-based flue gas sweetening unit
- Offshore CO_2 storage unit

the storage unit is modeled as a tank (TK-100) to represent the process interface, with costs per ton of CO_2 sourced from literature for economic analysis [25] and applied for comparison with the CCU scenarios. This approach enables a realistic cost evaluation while maintaining clarity and simplicity in the simulation model. The biogas feed (100 kgmol/h, CO_2 (66.97 wt%), CH_4 (31.15 wt%); Table S1) [26]. directly enters the amine-based upgrading unit.

2.2.1.1. Amine-based biogas upgrading unit. Fig. 1 illustrates the amine-based biogas upgrading unit. Raw biogas (stream 1: 2832 kg/h, 25 °C, 1 bar) is initially compressed to 2 bar ($K-100$) to enhance CO_2 absorption. The pressurized gas is then cooled in air cooler (E-101) to approximately 40 °C to optimize solvent contact conditions. It then enters the bottom of the 20-stage absorption tower (T-100), where it rises counter-currently to the descending MEA solvent (stream 13), introduced at the top at 45 °C and 1.8 bar.

This configuration, which consists of 20 theoretical stages with structured packing, ensures a CO_2 removal efficiency of 98%, reducing the CO_2 content in the treated biogas to below 3% by mass. The absorber's bottom temperature is maintained at 72.4 °C using partial solvent recycling and interstage cooling to manage the exothermic nature of the absorption process.

The CO_2-depleted biogas exits the top of the absorber (flow 16) and is subsequently recompressed in K-101 to 5.94 bar. It is then cooled to 25 °C (in heat exchanger E-103) before entering a two-phase separator (V-100), where condensed water is removed (WW-1). A second separator (V-101) further dries the gas stream (WW-2) already recompressed (in K-102) and cooled to 25 °C (in E-104), producing the final biomethane product (stream 20), which is described in Table S2.

This stream is delivered at 19.76 bar and 25 °C with a CH_4 purity exceeding 90%, making it suitable for entry into the CCPP. Meanwhile, the CO_2-rich MEA solution (stream 3) is pumped from 1 bar to 1.8 bar (by P-100) and preheated to 95 °C in the lean-rich heat exchanger (E-100) before entering the 15-tray stripper column (T-101). Operating at 1.2 bar at the bottom and 1.0 bar at the top, the stripper regenerates the solvent through thermal desorption. The released CO_2 (stream 9) exits from the column top for compression or storage, while the regenerated lean MEA (stream 7) is collected at the bottom, heat-exchanged with the rich feed, supplemented with makeup streams (MUW-1 and MUA-1) to compensate for losses, and recycled to the absorber at 45 °C.

2.2.1.2. Combined-cycle power generation (CCPP) unit. As illustrated in Fig. 2, purified biomethane (stream 20; 19.76 bar, 25 °C) fuels a gas turbine (G-100), where it combusts with (18 bar, 428.4 °C). The resulting high-temperature exhaust gases (stream 24, 1 bar and 1282 °C) drive a Heat Recovery Steam Generator (HRSG), successively producing high-, medium-, and low-pressure steam for a steam turbine (ST-100).

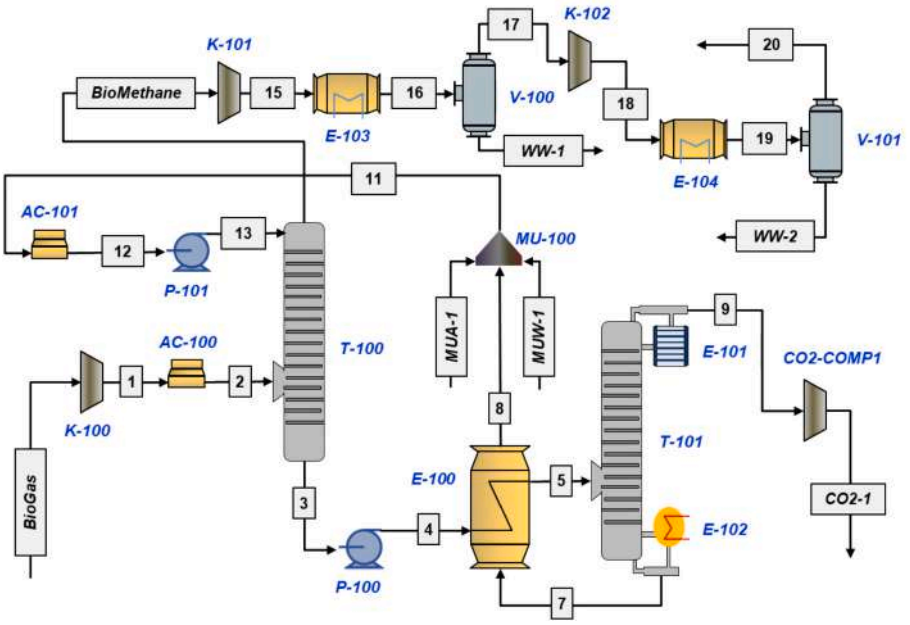

Fig. 1. Aspen HYSYS simulation model of the amine-based absorption unit for biogas upgrading.

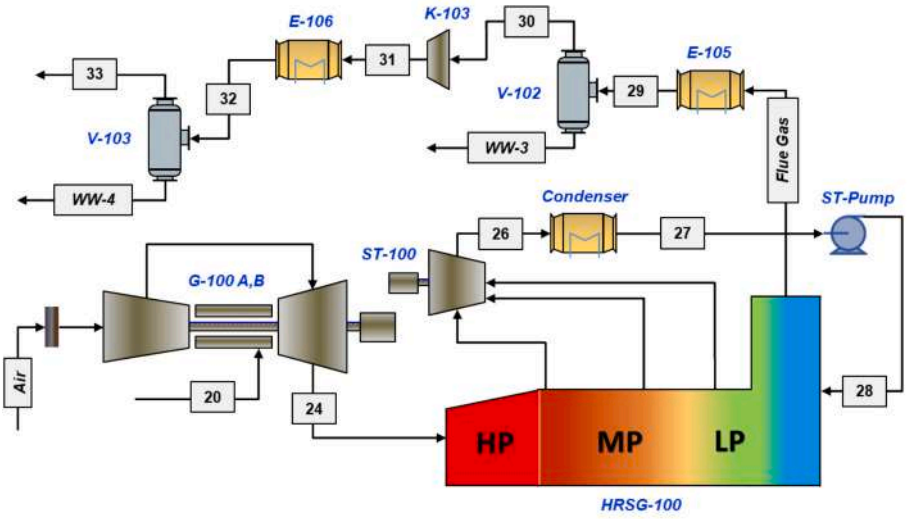

Fig. 2. Aspen HYSYS simulation model of the Combined-Cycle Power Plant (CCPP).

The combined mechanical work output from G-100 and ST-100 is converted into electricity through a shared generator, thereby maximizing the overall efficiency of the CCPP. Following expansion, the low-pressure steam exiting the steam turbine (stream 26, 0.068 bar and 38.7 °C) condenses in the condenser, and is then pumped back to the HRSG as feedwater (stream 28), completing the Rankine cycle. In parallel, the HRSG flue gas passes through two consecutive separators (V-102 and V-103), where condensed moisture is removed. The resulting dried flue gas is subsequently cooled and expanded to 2.6 bar and 25 °C (stream 33; see Table S3), after which it enters the CO_2 capture unit. At this stage, CO_2 is selectively removed using either amine-based absorption or membrane separation, depending on the configuration.

2.2.1.3. Amine-based flue-gas sweetening unit. As shown in Fig. 3, the dry flue gas stream (stream 33) is initially compressed (in compressor K-104) to 8.1 bar and 167.6 °C to increase the partial pressure of CO_2. The hot, compressed stream (stream 34) is cooled to 40 °C using air cooler (AC-102) and then further conditioned to the target absorption temperature in shell-and-tube exchanger (E-108) using cooling water.

The conditioned gas (stream 36) enters the bottom of the absorber column (T-102), a 20-tray tower operating at 1.2 bar at the top and 1.0 bar at the bottom. Inside the column, the gas ascends in counter-current contact with lean MEA solvent (stream 44), which is pumped by P-102. Selective CO_2 absorption occurs as the solvent reacts with the gas, producing a rich MEA solution (stream 41) at the column bottom. Simultaneously, the CO_2-depleted gas (stream 45) exits from the top, is cooled, and flashed to remove condensed moisture, yielding a high-purity nitrogen stream.

The rich MEA stream (stream 41) is preheated in the lean/rich heat exchanger (E-107) by exchanging heat with the hot lean MEA (stream 38), and then enters the stripper (T-103), which has 15 trays and operates at 1.3 bar at the bottom and 1.1 bar at the top. The reboiler (E-110) provides the required thermal energy to release CO_2 from the solvent. The resulting CO_2-rich vapor (stream 47) is condensed in E-109,

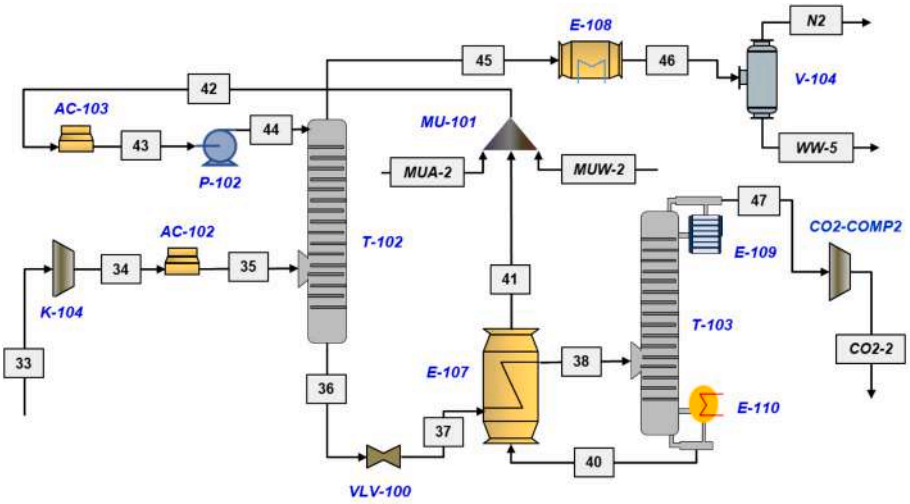

Fig. 3. Aspen HYSYS simulation model of absorption-based flue gas sweetening unit.

and the condensate is separated from the dry CO_2 (in separator V-104). The dry CO_2 stream is subsequently compressed (in CO_2-COMP2) to reach the desired pressure for either sequestration or utilization (stream CO_2–2). The regenerated lean MEA (stream 38) is routed back to the lean/rich exchanger E-107, cooled in air cooler (AC-103), supplemented with makeup water (MUW-2), and recycled to the absorber. This closed-loop configuration ensures minimal solvent loss and maximizes thermal integration between the absorber and the stripper.

2.2.2. *Membrane-based CCS units integrated with biogas fired power plant (MB-CCS)*

Fig. S3 presents the PFD of the MB-CCS configuration, which includes:

- Membrane-based biogas upgrading unit
- CCPP unit (Section 2.2.1.2)
- Membrane-based flue gas sweetening unit
- Offshore CO_2 storage unit

Consistent with the approach in Section 2.2.1, the offshore CO_2 storage unit was not simulated in this configuration and was considered solely for comparative economic analysis. Similarly, the feed conditions remain identical to those of the conventional case and are provided in Table S1.

2.2.2.1. Membrane-based Biogas Upgrading. As illustrated in Fig. 4, the two-stage carbon molecular sieve (CMS) membrane system is employed to upgrade raw biogas and meet fuel specification requirements. The feed gas is initially compressed and subsequently cooled to 19.90 bar and 55 °C (stream 7), and then introduced into the first membrane module (M-100). These conditions ensure the accuracy of performance data and alignment with the membrane model used. Under a trans-membrane pressure of 19.47 bar, CO_2 selectively permeates through the membrane, while the methane-enriched retentate (stream R1) exits the module and is directed to the CCPP. The composition and operating conditions of this retentate are summarized in Table S4. The permeate stream from the first stage (stream P1) is recompressed to 19.93 bar and cooled to 55 °C before entering the second membrane module (M-101). A transmembrane pressure gradient of 19 bar facilitates further CO_2 separation, yielding a high-purity CO_2 stream (stream P2) suitable for

Table 1
Gas permeance of the CMS membrane used for biogas upgrading at 55 °C [27].

Components	Permeance (GPU)
CO_2	193.00
N_2	1.07
CH_4	0.49

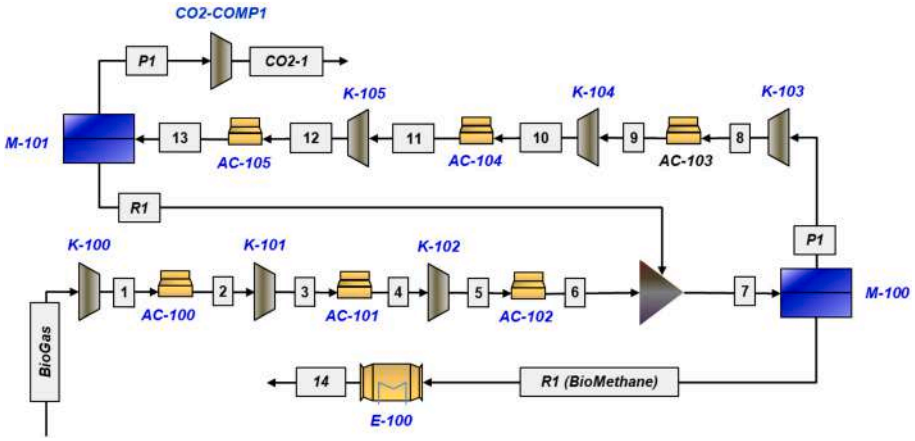

Fig. 4. Aspen HYSYS simulation model of the membrane-based biogas upgrading unit.

storage or utilization.

A portion of the retentate from M-101 (stream R2) is recycled to M-100 to enhance overall methane recovery and ensure stable separation performance. The permeance of the CMS membrane for biogas upgrading at 55 °C is presented in Table 1, where the values for CO_2, N_2, and CH_4 are 193, 1.07, and 0.49 GPU, respectively. This two-stage membrane system reduces the CO_2 content of the upgraded biogas to 1–3%, meeting CCPP fuel quality standards and ensuring sufficient methane for efficient combustion.

The membrane surface areas of modules M-100 and M-101 were calculated through an iterative design process to meet the methane purity requirements of the CCPP fuel while minimizing recompression energy. The first-stage module (M-100) was assigned a larger membrane area (1250 m^2) to handle the high CO_2 load of raw biogas and achieve bulk separation. In contrast, the second-stage module (M-101) functions as a polishing step and thus requires a significantly smaller area (150 m^2). Stage-cut values were maintained at moderate levels to prevent excessive methane loss in the permeate stream. The recycle stream from the second stage was introduced to enhance overall methane recovery while limiting additional compression duty and capital costs.

2.2.2.2. Membrane-based Flue-Gas Sweetening. As illustrated in Fig. 5, the dried flue gas stream exiting the CCPP (stream 27) is first compressed in compressor K-107 to 8.6 bar and 43.6 °C (stream 29). This high-pressure, elevated-temperature stream is mixed with two recycle streams (streams 46 and P5) to form feed stream 30, which is then directed to the first membrane module (M-102).

Under a transmembrane pressure of 8.5 bar, module M-102 separates a CO_2-rich permeate stream (stream P3) from an N_2-rich retentate stream (stream R3). The retentate continues to the second membrane stage (M-103), where additional CO_2 removal yields a high-purity nitrogen retentate. Meanwhile, the corresponding permeate stream (stream P4) passes through a series of three dehydration vessels (V-102, V-103, and V-104), each preceded by a dedicated compression and cooling step (K-111 to K-113 and AC-107 to AC-109, respectively). The resulting dry gas stream (stream 46) is recycled and reintroduced into the M-102 feed.

The permeate from M-102 (stream P3) is compressed in K-108 and cooled in AC-110 to reach 0.92 bar and 43.3 °C (stream 28). 70% of this stream (stream 33) is further compressed in K-103 and K-104 and cooled in AC-103 and AC-104 to 8.7 bar and 42.3 °C (stream 37), before being fed into the third membrane module (M-104). In this final stage, the retentate (stream R5) is combined with the remaining 30% sidestream (stream 47) to produce a high-purity CO_2 product (≥98 mol% CO_2). The M-104 permeate (stream P5) is recycled to the M-102 feed line, along with stream 46, thereby closing the membrane separation loop. The permeance of the CMS membrane for flue-gas sweetening at 45 °C is shown in Table 2, with CO_2 and N_2 values of 513 and 3.2 GPU, respectively.

Table 2
Gas permeance of the CMS membrane used for flue-gas sweetening at 55°C [27].

Components	Permeance (GPU)
CO_2	513.00
N_2	3.20

The membrane surface areas in the flue-gas sweetening unit were determined based on the high volumetric flow rate and low CO_2 concentration characteristic of CCPP exhaust gases. The first and second membrane stages (M-102 and M-103) each received a membrane area of 2558 m^2 to provide enough driving force for CO_2 separation while maintaining moderate stage-cut values and acceptable pressure ratios. These two stages mainly perform bulk CO_2 removal and nitrogen enrichment, respectively. The third membrane module (M-104), with a smaller membrane area of 234 m^2, acts as a final enrichment stage to achieve high-purity CO_2 suitable for storage or utilization. Stage-cut values were kept within moderate ranges to prevent excessive permeation, which could otherwise increase recompression duty and dilute retentate streams. Pressure drops across the membrane modules were assumed to be moderate and consistent with industrial CMS membrane systems, ensuring realistic compressor sizing without overestimating energy penalties.

Although the same class of CMS membranes was employed, the permeance values in Table 1 (CO_2/CH_4) and Table 2 (CO_2/N_2) differ significantly. This discrepancy primarily arises from the strong competitive sorption of CH_4 with CO_2 in biogas streams, which reduces the effective CO_2 permeance, whereas N_2 exhibits negligible sorption in flue gas, allowing CO_2 to permeate more readily. In addition, the membranes are structurally optimised for each application: in biogas upgrading, a thicker selective layer with narrower pores is designed to maximize CO_2/CH_4 selectivity at the expense of permeance, while in flue-gas sweetening, a thinner layer with more open pores enables higher CO_2 throughput.

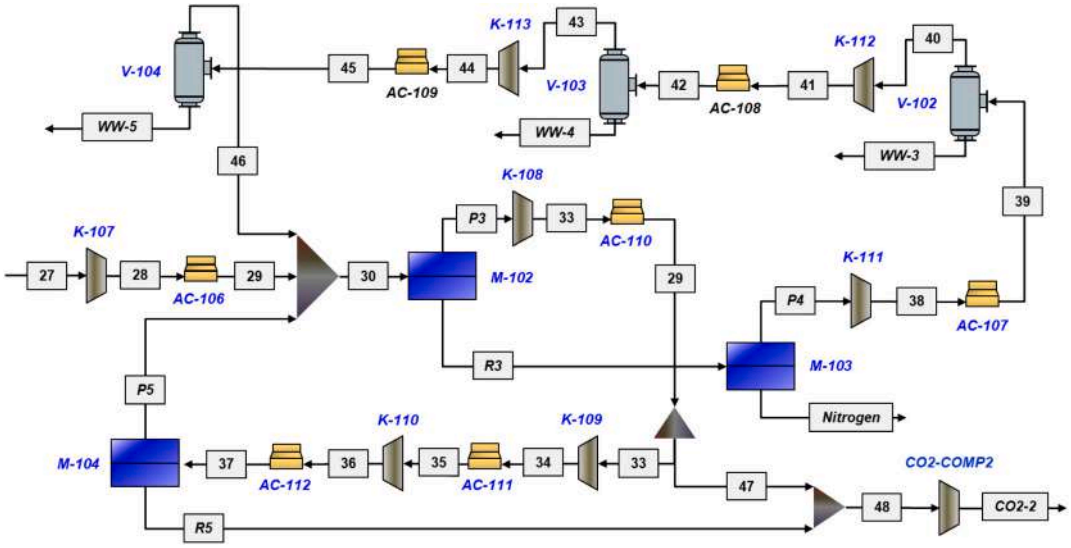

Fig. 5. Aspen HYSYS simulation model of the membrane-based flue gas sweetening unit.

2.3. Model development for integration of CCU schemes

2.3.1. Conventional CCU units integrated with a fired power plant (C-CCU)

Fig. S4 presents the process flow diagram (PFD) of the C-CCU configuration, which consists of five principal process units:

- Amine-based biogas upgrading unit (Section 2.2.1.1)
- CCPP unit (Section 2.2.1.2)
- Amine-based flue gas sweetening unit (Section 2.2.1.3)
- CO_2 hydrogenation reactor for fuel synthesis
- CO_2/H_2 recovery unit via amine absorption

Units 1, 2 and 3 are identical in design and modeling approach to those described under the C-CCS configuration and are not repeated here. Feed conditions are consistent with those summarized in Table S1.

2.3.1.1. Conventional CO_2 hydrogenation unit. As shown in Fig. 6, the three captured CO_2 streams: CO_2–1 from the amine upgrading unit, CO_2–2 from the amine sweetening unit, and stream 93 recycled from the CO_2 and H_2 recovery unit, are combined with hydrogen streams, namely stream 91 as recycled hydrogen and the makeup hydrogen stream labeled H_2 MU.

This combined feed (stream 49) is preheated in heat exchanger E-112 and then further heated in furnace F-100 to reach the reactor inlet conditions of 9.65 bar and 300 °C (stream 51). The heated mixture enters reactor R-100, a fixed-bed catalytic reactor containing Fe—K supported on γ-Al_2O_3. Under these operating conditions, CO_2 hydrogenation occurs, producing light alcohols and hydrocarbons, as described by the kinetic model presented in the following section. The reactor effluent (stream 52) is cooled in two successive heat exchangers before entering a series of three two-phase separators, identified as V-107, V-108, and V-109, for physical dehydration. The resulting dehydrated stream (stream 60) is subsequently directed to the CO_2 and H_2 recovery unit for final solvent-based purification, as described in Section 2.2.1.1. The operating conditions and mass composition of this stream are summarized in Table S5. The performance of reactor R-100 (see Fig. 6) is simulated based on the kinetic model developed by Najari et al. [28], which was experimentally validated for conditions up to 10 bar, 360 °C, and an H_2/ CO_2 molar ratio of 3.0. The model includes twelve elementary reactions, defined in Eqs. 1 to 12, with the corresponding kinetic parameters listed in Table 3 [29].

The units for the Arrhenius pre-exponential factor are kmol/(h·m^3·bar), and the units for the activation energy are kJ/kmol. To improve prediction accuracy under hydrogen-rich environments, a reversible expression is applied specifically to the highly exothermic methanation reaction, which was originally assumed to be irreversible. The remaining reaction rates retain their original irreversible formulations. This hybrid kinetic scheme enables accurate simulation of product distributions, including methane, C_2 to C_4 olefins such as ethylene and propylene, as well as heavier hydrocarbons, under the reactor's operating conditions of 9.65 bar and 300 °C. The model predicts total olefin yields of up to 50%.

Table 3
Kinetic rate expressions and parameters for CO_2 hydrogenation over Fe-K/γ-Al_2O_3 catalyst [29].

Reaction		
$CO_2 + H_2 \leftrightarrow CO + H_2$	$R_1 = 4.42 \times 10^{13}.\exp\left(\frac{-94850}{RT}\right).\frac{P_{CO_2}.P_{H_2} - P_{CO}.P_{H_2O}/K_{eq}}{P_{CO} + 53.47P_{H_2O} + 4.56\,P_{CO_2}}$	(Eq.1)
$CO + 3H_2 \rightarrow CH_4 + H_2O$	$R_2 = 5.29 \times 10^{13}.\exp\left(\frac{-135000}{RT}\right).\frac{P_{CO}.P_{H_2}}{P_{CO} + 43.05P_{H_2O} + 3.42P_{CO_2}}$	(Eq.2)
$2CO + 4H_2 \rightarrow C_2H_4 + 2H_2O$	$R_3 = 5.67 \times 10^{14}.\exp\left(\frac{-146000}{RT}\right).\frac{P_{CO}.P_{H_2}}{P_{CO} + 41.18P_{H_2O} + 3.11P_{CO_2}}$	(Eq.3)
$2CO + 5H_2 \rightarrow C_2H_6 + 2H_2O$	$R_4 = 6.83 \times 10^{13}.\exp\left(\frac{-141000}{RT}\right).\frac{P_{CO}.P_{H_2}}{P_{CO} + 85.93P_{H_2O} + 2.32P_{CO_2}}$	(Eq.4)
$3CO + 6H_2 \rightarrow C_3H_6 + 3H_2O$	$R_5 = 3.53 \times 10^{14}.\exp\left(\frac{-147100}{RT}\right).\frac{P_{CO}.P_{H_2}}{P_{CO} + 15.94P_{H_2O} + 4.05P_{CO_2}}$	(Eq.5)
$3CO + 7H_2 \rightarrow C_3H_8 + 3H_2O$	$R_6 = 1.97 \times 10^{12}.\exp\left(\frac{-127000}{RT}\right).\frac{P_{CO}.P_{H_2}}{P_{CO} + 55.56P_{H_2O} + 3.15P_{CO_2}}$	(Eq.6)
$4CO + 8H_2 \rightarrow C_4H_8 + 4H_2O$	$R_7 = 1.94 \times 10^{11}.\exp\left(\frac{-111000}{RT}\right).\frac{P_{CO}.P_{H_2}}{P_{CO} + 30.91P_{H_2O} + 4.95P_{CO_2}}$	(Eq.7)
$4CO + 9H_2 \rightarrow i - C_4H_{10} + 4H_2O$	$R_8 = 1.17 \times 10^{8}.\exp\left(\frac{-87000}{RT}\right).\frac{P_{CO}.P_{H_2}}{P_{CO} + 87.91P_{H_2O} + 3.74P_{CO_2}}$	(Eq.8)
$4CO + 9H_2 \rightarrow n - C_4H_{10} + 4H_2O$	$R_9 = 1.17 \times 10^{8}.\exp\left(\frac{-87000}{RT}\right).\frac{P_{CO}.P_{H_2}}{P_{CO} + 87.91P_{H_2O} + 3.74P_{CO_2}}$	(Eq.9)
$2CO_2 + 6H_2 \rightarrow C_2H_4 + 4H_2O$	$R_{10} = 5.07 \times 10^{7}.\exp\left(\frac{-150000}{RT}\right).\frac{P_{CO_2}.P_{H_2}}{P_{CO} + 73.34P_{H_2O} + 62.02P_{CO_2}}$	(Eq.10)
$3CO_2 + 9H_2 \rightarrow C_3H_6 + 6H_2O$	$R_{11} = 5.07 \times 10^{7}.\exp\left(\frac{-150000}{RT}\right).\frac{P_{CO_2}.P_{H_2}}{P_{CO} + 73.34P_{H_2O} + 62.02P_{CO_2}}$	(Eq.11)
$4CO_2 + 12H_2 \rightarrow C_4H_8 + 8H_2O$	$R_{12} = 5.07 \times 10^{7}.\exp\left(\frac{-150000}{RT}\right).\frac{P_{CO_2}.P_{H_2}}{P_{CO} + 73.34P_{H_2O} + 62.02P_{CO_2}}$	(Eq.12)

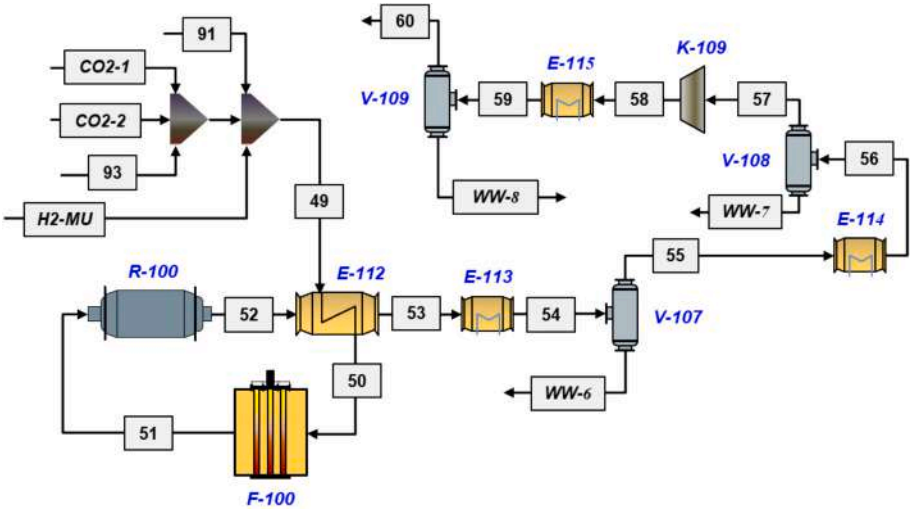

Fig. 6. Aspen HYSYS simulation model of Conventional CO_2 Hydrogenation Unit.

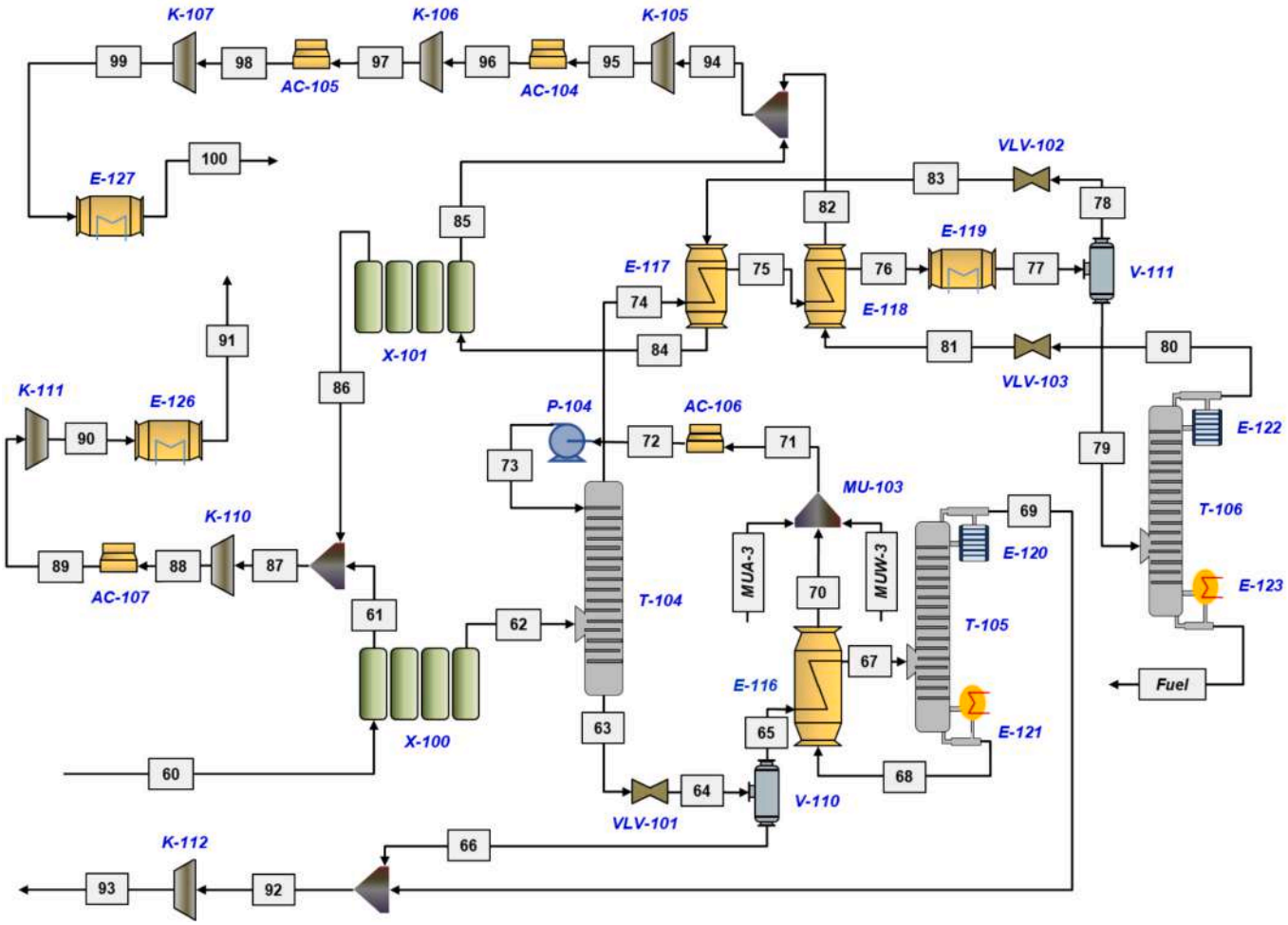

Fig. 7. Aspen HYSYS simulation model of conventional CO_2 & H_2 recovery unit.

2.3.1.2. Conventional CO_2/H_2 recovery unit. The product stream from the CO_2 hydrogenation unit contains unreacted H_2 and CO_2. The primary objective of the CO_2/H_2 recovery unit is to recover these components and upgrade the fuel product. As illustrated in Fig. 7, the dried product stream (stream 60) from the CO_2 hydrogenation reactor enters a pressure swing adsorption (PSA) column (X-100) for hydrogen adsorption. The high-purity hydrogen stream (stream 61) is then combined with another hydrogen stream (stream 86) from a second PSA column (X-101). This combined stream is pressurized using a two-stage compressor ($K-110$,$K-111$) and subsequently passes through a heat exchanger (E-126), reaching 10 bar and 39 °C before being recycled to the CO_2 hydrogenation unit. The remaining output from the first PSA column (stream 62) is directed to an absorption tower (T-104) for CO_2 capture. In this tower, the gas stream (stream 62) comes into countercurrent contact with the MEA solvent (stream 73) across multiple trays. The stripped CO_2 gas stream (stream 74) exits from the top of the tower and, after passing through three heat exchangers and a two-phase separator operating at −90 °C and 29.89 bar, is routed to a distillation column (T-106) for further purification.

The bottom product of the absorption tower (stream 63), which is an MEA-rich CO_2 stream, is sent to another distillation column (T-105) for solvent regeneration. The recovered MEA is then recycled back to the absorption tower.

In the distillation column T-105, the top product gas stream (stream 69), which is rich in CO_2, is mixed with a dried stream (stream 66) from the two-phase separator (V-110). This combined stream is recycled to the CO_2 hydrogenation unit as stream 93, at 10 bar and 221 °C. Simultaneously, in distillation column T-106, the treated fuel gas stream (stream 79) is separated into heavy hydrocarbons, which exit as the main product (stream Fuel), and light hydrocarbons, which exit as the top product stream (stream 80), as detailed in Table S6. Stream 80, after passing through a pressure relief valve and heat exchanger (E-118), is combined with stream 85 to form stream 94, at 1 bar and 21.49 °C.

Stream 94 then undergoes a three-stage compression and cooling process, resulting in an enriched methane stream (stream 100) at 18 bar and 25 °C, which is subsequently recycled to the CCPP. Additionally, the second PSA column (X-101) is used to recover residual hydrogen from the top product of the absorption tower. After preliminary treatment, this stream (stream 84) enters PSA column X-101, where an enriched H_2 stream (stream 86) is produced and combined with the hydrogen recovered from the first PSA column (stream 61), as described earlier.

2.3.2. Membrane-based CCU units integrated with biogas fired power plant (MB-CCU)

Fig. S5 presents the PFD of the MB-CCU configuration, which consists of five principal process units:

- Membrane-based biogas upgrading unit (Section 2.2.1.4)
- CCPP unit (Section 2.2.1.2)
- Membrane-based flue gas sweetening unit (Section 2.2.1.5)
- Membrane reactor for CO_2 hydrogenation to liquid fuels
- Membrane-based CO_2/H_2 recovery unit

Units 1–3 are identical in design and modeling approach to those

described under the MB-CCS configuration and are not repeated here. Feed conditions are consistent with those summarized in Table S1.

In the proposed membrane-based CCU (MB-CCU) setup, the flue-gas sweetening unit was redesigned to accommodate the increased gas throughput resulting from internal recycle streams for CO_2 and CH_4 recovery and utilization. Compared to the MB-CCS version, higher recycle ratios and additional circulating gas flows resulted in increased volumetric flow rates into the flue-gas membrane separation train. Consequently, larger membrane surface areas were required for modules M-102 and M-103 (each 3709.1 m^2) and for the final enrichment module M-104 (339.3 m^2) to maintain similar separation performance, moderate stage-cut levels, and acceptable pressure ratios. This design modification ensures that integrating the CCU does not reduce CO_2 capture efficiency and prevents excessive energy penalties from recompression. Meanwhile, the membrane-based biogas upgrading unit remains unchanged from the MB-CCS setup, as the biogas feed composition and flow rate are the same in both cases.

It is worth noting that combining a membrane reactor with a membrane-based separation unit for the simultaneous recovery of H_2 and CO_2 represents a relatively new process configuration. This setup has been specifically designed in this work to enable integrated reaction–separation functionality tailored for CCU applications.

2.3.2.1. Membrane-based CO_2 hydrogenation unit. In the newly proposed configuration illustrated in Fig. 8, a membrane reactor (MR) is used to facilitate CO_2 hydrogenation.

This reactor integrates a H_2O-selective sodalite membrane (as specified in Table 4) to remove water from the reaction zone selectively. This selective permeation shifts the reaction equilibrium toward the product side in accordance with Le Chatelier's principle.

In the MB-CCU scheme, this reactor receives two CO_2-rich streams, labeled CO2–1 and CO2–2, which are captured from membrane-based biogas upgrading and flue gas sweetening units, respectively. These streams are blended with recycled stream 71 (see Table S7), which contains a hydrogen-carbon dioxide mixture obtained from the membrane-based CO_2 and H_2 recovery unit, supplemented with a hydrogen makeup stream (H_2-MU) to optimize the hydrogen-to-carbon dioxide ratio at the reactor inlet. The resulting mixed stream, denoted as stream 52 (refer to Table S8), is then preheated using a heat exchanger (E103) and a furnace (F100) to a pressure of 10 bar and temperature of 300 °C (stream 54) before entering the sodalite membrane reactor (R-100 (MR)).

Table 4
The sodalite membrane specifications used in the unit simulation [30].

Components	Permeance (L(STP)/m^2•h•bar)
H_2O	4034
H_2	403
CO	134
CO_2	134

The output stream is then directed to the membrane-based CO_2 and H_2 recovery unit for further purification. At the same time, the permeate stream (stream 54) is compressed in a two-stage compression system and sent through two phase separators for steam recovery. The treated permeate is recycled and merged with the incoming H_2-CO_2 mixture at the reactor inlet as stream 62 under the same operating conditions (10 bar, 131.7 °C). The reactor simulation uses the same kinetic model as the conventional reactor.

The surface area of the sodalite membrane integrated into the membrane reactor was determined based on the required water-removal rate needed to effectively shift the reaction equilibrium toward products while maintaining stable reactor operation. A membrane area of 1260 m^2 was selected to ensure sufficient H_2O permeation under the specified operating conditions, without inducing excessive reactant loss or additional compression requirements. To account for component transport across the membrane [31], a source or sink term is included in the model. This term is defined by Eq. (13):

$$S_i = \frac{A \bullet J_i \bullet M_i}{V} \tag{13}$$

The permeation flux Ji is calculated based on Eq. (14):

$$J_i = P_{ei}\left(P_{i,retentate} - P_{i,permeate}\right) \tag{14}$$

where J_i ($mol \cdot m^{-2} \cdot s^{-1}$) is the membrane permeation flux of component *i*, $P_{e,i}$ ($mol \cdot m^{-2} \cdot s^{-1} \cdot Pa^{-1}$) and $P_{i,retentate}$ and $P_{i,permeate}$ are the partial pressures of component *i* on the retentate and permeate sides, respectively. This approach enables accurate prediction of conversion and selectivity in the membrane reactor by enhancing water removal and driving the reaction forward.

2.3.2.2. Membrane-based CO_2/H_2 recovery unit. In the MB-CCU configuration, as in the conventional approach, the product stream exiting the

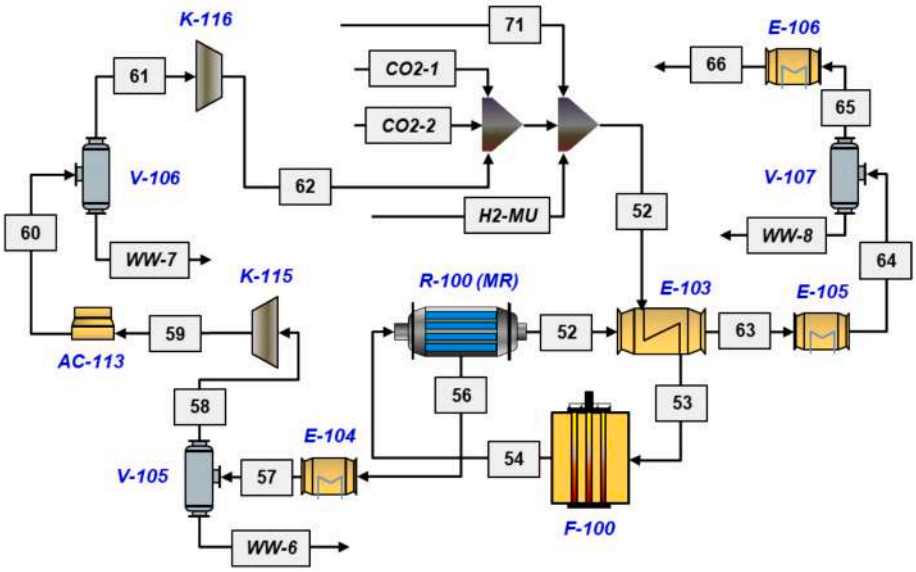

Fig. 8. Aspen HYSYS simulation model of a membrane-based CO_2 hydrogenation unit.

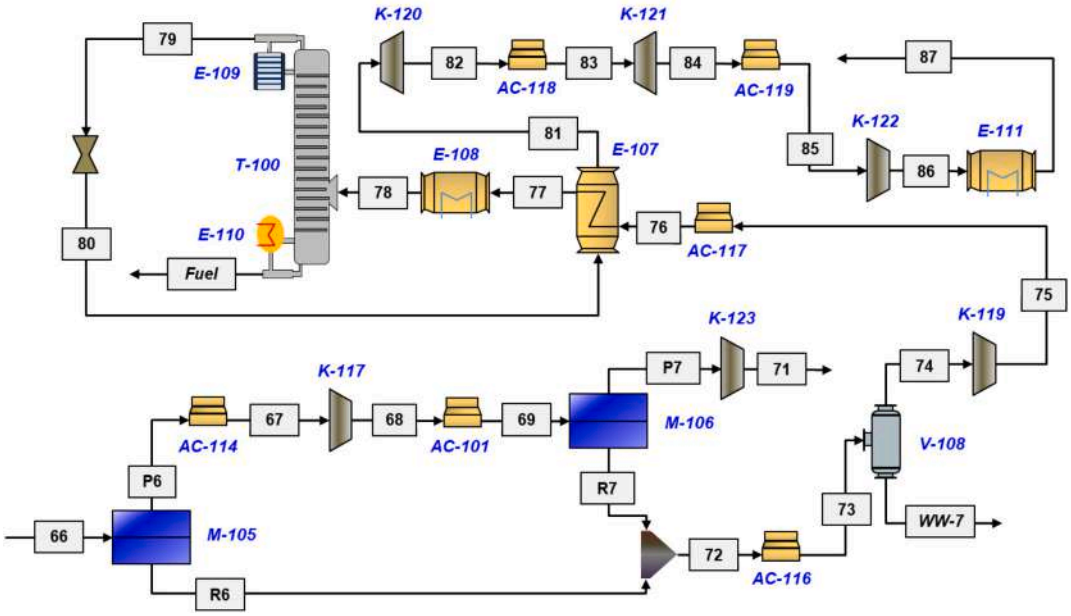

Fig. 9. Aspen HYSYS simulation model of a membrane-based CO_2 & H_2 recovery unit.

CO_2 hydrogenation unit requires recovery of unreacted CO_2 and H_2, as well as upgrading of the generated hydrocarbon fuels. This is achieved through a hybrid separation process illustrated in Fig. 9, which combines a two-stage membrane system with a distillation column. The membrane separation system comprises two silica-based membrane modules, M-105 and M-106, configured as proposed by Ghasemzadeh et al. [28]. These membranes are microporous ceramic types designed explicitly for H_2 and CO_2 separation, and their detailed specifications are listed in Table 5.

Initially, stream 66 enters membrane module M-105, where selective permeation of H_2 and CO_2 occurs. The permeate stream (stream P6) is cooled in the air cooler AC-114, compressed by compressor K-117, and further cooled in AC-101 to reach the specified operating conditions of 2.8 bar and 42.44 °C (stream 69). This treated stream is then fed into the second membrane module (M-106) for enhanced purification of permeate components.

The retentate stream from M-106 (stream R7) is combined with the retentate from M-105 (stream R6) to form stream 72, which is directed to the next stage of processing. Simultaneously, the permeate stream from M-106 is compressed to 1 bar and 195 °C (stream 71) and recycled back to the membrane-based CO_2 hydrogenation unit, thereby minimizing reactant loss and enhancing system efficiency.

The membrane surface areas of modules M-105 and M-106 were chosen to accommodate the increased flow rates and component recycling inherent to the MB-CCU system. Module M-105, with a membrane area of 2100 m^2, is designed to handle the higher inlet flow rate of the reactor effluent and to carry out bulk separation of H₂ and CO_2. Conversely, the second-stage module M-106 functions as a polishing step, requiring a smaller membrane area of 550 m^2 to reach the desired permeate purity for recycling to the membrane reactor. The permeate stream from M-106 is recycled back to the membrane-based CO_2 hydrogenation reactor to minimize hydrogen and CO_2 losses and improve overall carbon utilization efficiency. The selected membrane areas enable this recycle stream to be maintained at moderate flow rates, thereby avoiding excessive recompression work while preserving reactor feed composition and pressure. This integrated design guarantees reactant recovery and reuse without compromising the economic performance of the MB-CCU system. Stage-cut values in both membrane modules were kept within moderate limits to prevent excessive permeation, which could otherwise increase compression energy requirements and dilute the retentate streams.

Table 5
The silica membrane specifications used in the unit simulation [32]

Components	Permeance (L(STP)/m^2•h•bar)
H_2	4015
CO	807
CO_2	807
CH_4	40
N_2	50

The combined retentate stream (stream 72) is subsequently cooled using AC-116 and then passed through a two-phase separator to remove water. The resulting dried stream is compressed and directed through two heat exchangers (E-107 and E-108) before entering a distillation column (T-100), configured as a de-methanizer, to separate methane from heavier hydrocarbon components. The preheated stream (stream 78) enters the distillation column at 28.81 bar and − 90 °C. The overhead product (stream 79) undergoes pressure reduction using a relief valve, followed by cooling in E-107, a three-stage compression and cooling sequence, and final conditioning in E-111. The resulting stream 87, at 19.7 bar and 25 °C, is a methane-rich stream that is recycled to the CCPP for fuel reuse. Meanwhile, the bottom product from the distillation column (stream fuel) is considered the final upgraded hydrocarbon fuel. It represents the saleable output of the CO_2 hydrogenation section within the MB-CCU configuration.

2.4. Economic assessment

An economic analysis was conducted to compare two carbon management strategies, CCS and CCU, in biogas-fueled CCPPs, evaluating both membrane-based and conventional capture approaches. The capital expenditures were estimated by calculating the total equipment cost (TEC) using empirical cost correlations for major process and auxiliary units. Installation factors were then applied to obtain the total installed cost (TIC) [33]. Equipment exposed to corrosive environments was assumed to be constructed from 304 stainless steel (material factor = 1.3) [34], whereas the rest was assumed to be constructed from carbon steel (material factor = 1.0) [25]. All correlations were updated to 2025 economic conditions using the Chemical Engineering Plant Cost Index (CEPCI = 800.2) [35]. Table 6 summarizes the cost-estimation equations

Table 6
Equipment cost correlations and associated installation factors (updated to 2025 prices).

Equipment	Cost Eq. (2025)	Installation Factor	Ref.
Adsorption Packages	C_e (m$) = 0.25 × (kmole/h)$^{0.6}$	1.1	[36]
Air Cooler	C_e (m$) = 4.1 × 10^{-2} × (m^2)$^{0.4}$	2.5	[37]
Column	C_e (m$) = 0.027 + (1.2 × 10^{-4} × (kg)$^{0.85}$) + N× (1.9 × 10^{-4} + 6.6 × 10^{-4} (m)$^{1.8}$)	4	[38]
Combustion Turbine	C_e (m$) = 4 × 10^{-4} × (kW)	1.3	[39]
Compressor (Blower)	C_e (m$) = 6.7 × 10^{-3} + (8.6 × 10^{-5} × (m^3/h)$^{0.8}$)	2.5	[38]
Compressor (Centrifugal)	C_e (m$) = 0.9 + (0.03 × (kW)$^{0.6}$)	2.5	[38]
Compressor (Reciprocating)	C_e (m$) = 0.4 + (4.1 × 10^{-3} × (kW)$^{0.75}$)	2.5	[38]
Heat Exchanger (Double Pipe)	C_e (m$) = 2.9 × 10^{-3} + (3.8 × 10^{-3} × (m^2))	3.5	[38]
Heat Exchanger (Shell & Tube)	C_e (m$) = 4.8 × 10^{-2} + (1.1 × 10^{-4} × (m^2)$^{1.2}$)	3.5	[38]
HRSG and Ducting	C_e (m$) = 2 × 10^{-4} × (kW)	1.3	[39]
Kettle Reboiler	C_e (m$) = 4.4 × 10^{-2} + (6 × 10^{-4} × (m^2)$^{0.9}$)	3.5	[38]
Membrane Module + Frame Cost	C_e (m$) = ($\alpha_{TRL}$ + 1)) × 1 × 10^{-4} (m^2) + (9 × 10^{-3} × (m^2)$^{0.88}$)(	1.01	[27]
Pump	C_e (m$) = 0.01 + (3.6 × 10^{-4} × (Lit/s)$^{0.9}$) + (3 × 10^{-3} × (kW)$^{0.6}$)	4	[38]
Pressure Vessel (Horizontal)	C_e (m$) = 0.019 + (1.1 × 10^{-4} × (kg)$^{0.85}$)	4	[38]
Pressure Vessel (Vertical)	C_e (m$) = 0.027 + (1.2 × 10^{-4} × (kg)$^{0.85}$)	4	[38]
Reactor	C_e (m$) = 1.37 × (m^3)$^{0.85}$	2.5	[38]
Syngas Unit	C_e (m$) = 0.075 + (0.038 × (MMSCFD)$^{0.8}$)	2	[40]

and installation multipliers used in this study.

These equations are tailored to various equipment categories, such as compressors, heat exchangers, columns, and membrane modules, and reflect realistic industrial-scale-up behavior.For technologies with lower Technology Readiness Levels (TRLs), a percentage-based adjustment factor, denoted as α_{TRL}, must be added to the base equipment cost to account for technical uncertainty. According to IEAGHG (2021) [41], process contingency factors increase significantly at lower TRL values, exceeding 60% for TRL 3, ranging from 20% to 60% for TRL 4 to 6, and between 10% and 20% for TRL 7 to 8, while declining to 0–10% at TRL 9. This reflects the inverse relationship between technological maturity and capital cost uncertainty. Chemical absorption using aqueous amines is currently the most mature CO_2 capture technology, operating at TRL 9 with widespread commercial application.

Adsorption and cryogenic methods have also reached TRL 7 to 9, but remain limited by material and energy constraints. In contrast, membrane-based CO_2 separation is still at TRL 6 and requires further improvements in selectivity and permeance for large-scale deployment [42]. Membrane reactor technologies operate at TRL 5 to 6, reflecting successful pilot demonstrations; thus, a TRL-based cost multiplier should be applied [43]. The Battery Limits Investment (BLI) was determined as the aggregate of the TEC, TIC, and a contingency allowance. A contingency factor equal to 25% of the TIC was included to account for potential unforeseen expenditures and design-related uncertainties, as recommended by standard cost estimation practices [33]. Subsequently, the Total Fixed Capital (TFC) was calculated by adding the BLI to offsite costs, which encompass infrastructure, utility systems, and general service facilities located beyond the battery limits of the process area [24]. To quantify the Total Working Capital (TWC), a value equivalent to 25% of the TFC was assumed, reflecting the initial capital required to support plant operation, including raw material procurement, inventory buildup, and accounts receivable. Finally, the Total Capital Investment (TCI), representing the full financial requirement for plant construction, commissioning, and startup, was obtained by summing the TFC and

Table 7
Unit prices of key raw materials and utilities for techno-economic analysis (2025).

Name	Unit Price	Unit	Ref.
Biogas	6.8	USD/MWh	[47]
Natural Gas (SynGas Fees & Fuel)	17.1	USD/MWh	[48]
CO_2 Tax	50.0	USD/t	[49]
45Q Tax Credit	85.0	USD/t	
Cooling Water	0.1	USD/t	[50]
High Pressure (HP) Steam (Byproduct Sale)	10.0	USD/t.	[50]
Low-Pressure (LP) Steam	6.0	USD/t	[50]
Nitrogen-rich utility gas	15.0	USD/t	[51]
Electricity (Main Product Sale)	120.0	USD/MWh	[52]
Refrigerant	30.7	USD/MWh	[29]
Fuel	450.0	USD/t	[48]

TWC [24]. Operating expenditure (OPEX) is calculated in three steps. First, the 2025 base-year unit prices for raw materials, labour, utilities, and plant overhead (Table 7) are escalated at the assumed annual inflation rate of 2.5% [44,45]. Second, these inflation-adjusted cost streams are summed and reduced by the credit for the CO_2 tax avoided through on-site capture. Third, the following items are added: (i) the statutory carbon levy on indirect emissions, (ii) the cost of transporting and storing the captured CO_2, and (iii) the annual insurance charge, set at 2% of the TFC and indexed to inflation [46]. This procedure yields a coherent nominal OPEX profile that is fully consistent with the financial assumptions and is suitable for subsequent LCOE calculation. The LCOE represents the total cost of generating electricity, expressed in constant USD/MWh.

It is calculated by adding inflation-adjusted OPEX, book depreciation, and a fixed-percentage corporate overhead (including G&A, sales, and R&D) to the levelized capital charge, which refers to the annualized form of the initial fixed capital investment. After subtracting the nitrogen by-product credit, the discounted sum of these annual values is divided by the discounted lifetime net-electric output, yielding a single, comparable cost metric for power-generation technologies.

Finally, the model will quantify all key performance indicators required for a complete economic appraisal, including the total NPV, internal rate of return (IRR),(PBP, the LCOE in both USD/MWh and

Table 8
Technical KPIs for the techno-economic assessment [33,54].

Parameter	Unit	Equation
Chemical Efficiency (CE)	–	$CE = \frac{\dot{m}_{fuel}.LHV_{Lfuel}}{\dot{m}_{BG} \bullet LHV_{BG}}$
BioGas Demand (BGD)	–	$BGD = \frac{\dot{m}_{BG} \bullet LHV_{BG}}{P_{net}}$
Cooling Water Demand (CWD)	–	$CWD = \frac{Q_{CW}}{P_{net}}$
LP Steam Demand (LPSD)	–	$LPSD = \frac{Q_{LPS}}{P_{net}}$
HP Steam Demand (HPSD)	–	$HPSD = \frac{Q_{HPS}}{P_{net}}$
Furnace Fuel Demand (FFD)	–	$FFD = \frac{Q_{FF}}{P_{net}}$
Refrigerant Demand (RD)	–	$RD = \frac{Q_{REF}}{P_{net}}$
Total Energy Demand (TED)	–	$TED = \frac{Q_{Total}}{P_{net}}$
Generated CO_2 (PCO_2)	t/MWh	$GCO_2 = \frac{\dot{m}_{generated\ CO2}}{P_{net}}$
Specific Residence Time (SRT)	min/MW	$SRT = \frac{\tau}{P_{net}}$
N_2 Rich Output (NRO)	t/MWh	$NRO = \frac{\dot{m}_{N2}}{P_{net}}$
Fuel Output (FO)	t/MWh	$FO = \frac{\dot{m}_{Fuel}}{P_{net}}$
Wastewater Output (WO)	t/MWh	$WO = \frac{\dot{m}_{waste\ water}}{P_{net}}$

Table 9
Comparison of Reference and Simulated Advanced Technology Outputs: Final Outlet Composition, Total Flow, and Net Power [29].

Parameter	Unit	Reference	Simulation	Absolute Error	Relative Error (%)
• N_2 fraction	%	73.4	73	− 0.40	− 0.55
• O_2 fraction	%	13.68	13.6	− 0.08	− 0.58
• CO_2 fraction	%	6.09	6.05	− 0.04	− 0.66
• H_2O fraction	%	5.58	5.52	− 0.06	− 1.07
• Ar fraction	%	1.26	1.27	0.01	0.79
• CH_4 fraction	%	0	0	0	0.00
Total Flow (Stream 9)	lb/h	5,598,285	5,550,000	−48,285	− 0.86
Net Power (Advanced)	MW	460	446.2	−13.8	− 3.00

MUSD/Year, and the levelized cost of net carbon (LCNC, USD. ton^{-1} CO_2), and the annual net profit.

2.5. Technical performance indicators

A concise set of key performance indicators (KPIs) has been defined to benchmark conventional and membrane-based CCS and CCU configurations in biogas-fired combined-cycle power plants. As outlined in Table 8, these indicators are categorized into three dimensions: conversion efficiency, defined as the ratio of the fuel's chemical energy converted into net electric power; resource intensity, which accounts for the specific consumption of biogas, cooling water, LP and HP steam, furnace fuel, refrigerant, and overall energy per unit of net output; and system outputs, encompassing both the net carbon dioxide emissions (direct and indirect) and secondary by-products such as wastewater and nitrogen-rich streams. This structured framework directly links resource consumption, system outputs, and operating costs, providing a consistent base for comparing CCS and CCU scenarios.

3. Results and discussion

3.1. Model comparison with literature data

The biogas upgrading and flue gas sweetening data were fully validated against published data, following the work done by Cavaignac et al. [53] (see Supplementary Tables S9 - S11). For the conventional amine-based biogas upgrading unit, the key stripper performance metrics (reboiler heat duty and HHV) yielding a match within 1% of the values from the literature.

At the absorber outlet, the CH_4 and N_2 mass fractions show deviations of approximately 1.2% and − 4.6%, respectively, while the trace components (CO_2, CO, H_2S, and H_2O) exhibit relative errors in the range of 10–20%. These deviations for trace species, which are present only in very small concentrations (ppm level), are amplified in percentage terms but remain negligible with respect to overall process performance.

The membrane-based flue gas sweetening unit, as investigated by Rahimalimamaghani et al. [27], showed excellent agreement with the reference data. The deviations between our simulation and the reported values were less than 1.2% for the total membrane surface areas, under 1.6% for the overall permeate flow rates, and below 2% for the outlet gas compositions (CH_4, CO_2, and N_2) in the membranes.

Similarly, the combined-cycle power plant model, following IHS Markit [39], matched advanced technology reference values to within 1% for gas compositions and 3% for net power output (Table 9).

Finally, the CO_2 hydrogenation reactor simulation, based on Do and Kim [29], reproduced all Stream 3 values exactly and Stream 4 component flows within a maximum relative error of 3.33% (Table 10). Taken together, these results confirm that each unit operation has been modeled with very high accuracy and can be used with confidence for subsequent process analysis. The detailed explanations and supplementary discussion related to Tables 9 and 10 are provided in the Supplementary Information file.

3.2. Technical comparison of CCPPs

The key process stream specifications for the four configurations investigated in this study are presented in Tables S12-S15. These tables summarize the simulation results for the C-CCS, MB-CCS, C-CCU, and MB-CCU systems. For each primary stream, essential parameters are reported, including vapor fraction, temperature (°C), pressure (bar), mass flow rate (kg/h), molar flow rate (kgmol/h), heat flow (kcal/h), and component composition in mole fractions. These data are crucial for economic analysis, evaluating unit performance, and validating the process models across different carbon capture and utilization scenarios.

Fig. 10 presents the distribution of total energy consumption by energy type, including cold utilities, hot utilities such as steam and fuel, and electric power across the four modeled configurations. In the C-CCS system, hot and cold utilities dominate the energy profile, accounting for 33% and 55% of the total demand, respectively. This is primarily attributed to the extensive use of LP steam in the biogas upgrading and flue gas sweetening units, along with significant cooling requirements in the combined cycle power plant. In contrast, the MB-CCS configuration eliminates all hot utility consumption, resulting in a sharp shift toward cold energy (76%) and electrical power (24%). This transition reflects the replacement of steam-based solvent regeneration with membrane-based separations, which rely heavily on gas compression and cooling.

A similar trend is observed in the transition from conventional to MB-CCU systems. The C-CCU pathway exhibits a balanced but resource-intensive energy profile, with 71% cold, 22% hot, and 7% electric power contributions. The demand for hot utilities remains high due to steam consumption in the CO_2/H_2 recovery section and furnace heating in the CO_2 hydrogenation unit. However, in the MB-CCU system, the energy profile becomes overwhelmingly dominated by cold utilities (83%), with reduced shares of hot (5%) and power (12%) utilities. This reflects the minimization of thermal input through electrified separations and the use of refrigerant-based recovery systems. Overall, the analysis highlights a fundamental shift from thermal to mechanical and cooling utilities as membrane technologies are integrated, with implications for system design, energy sourcing, and the operational cost structure.

Fig. 11 illustrates the unit-wise distribution of total energy consumption across the four configurations. In C-CCS, energy demand is relatively balanced among the combined cycle power plant (49%), flue gas sweetening unit (30%), and biogas upgrading unit (21%), reflecting the combined impact of cooling and steam utilities. However, in the MB-CCS system, energy is highly concentrated in the power plant (83%), whereas contributions from upgrading and sweetening units decline sharply due to the elimination of steam use and the reliance on compression and cooling.

In the C-CCU, energy consumption is more evenly distributed, with the CO_2 hydrogenation unit (49%) as the primary consumer due to its intensive cooling and fuel requirements. The recovery and power units also contribute significantly. In contrast, MB-CCU exhibits a highly centralized energy profile, with the hydrogenation reactor alone accounting for 64% of total energy demand, whereas the recovery and sweetening units consume minimal energy. This shift toward energy

Table 10
Validation of CO_2 Hydrogenation Reactor Stream Compositions and Flows.

Stream	T (°C)	P (bar)	Component	Unit	Reference	Simulation	Absolute Error	Relative Error (%)
3	300	10	Total Flow	kmol/h	318,350	318,350	0	0
			CO_2	kmol/h	77,630	77,630	0	0
			H_2	kmol/h	236,588	236,588	0	0
			O_2	kmol/h	0	0	0	0
			H_2O	kmol/h	0.00%	0	0	0
			CO	kmol/h	1755	1755	0	0
			CH_4	kmol/h	351	351	0	0
			C_2H_4	kmol/h	951	951	0	0
			C_2H_6	kmol/h	86	86	0	0
			C_3H_6	kmol/h	731	731	0	0
			C_3H_8	kmol/h	51	51	0	0
			C_4H_8	kmol/h	176	176	0	0
			C_4H_{10}	kmol/h	32	32	0	0
			C_5^+	kmol/h	0.00%	0	0	0
4	300	10	Total Flow	kmol/h	295,889	300,000	4111	1.39
			CO_2	kmol/h	60,724	61,500	776	1.28
			H_2	kmol/h	192,592	195,000	2408	1.25
			O_2	kmol/h	0	0	0	0
			H_2O	kmol/h	29,534	3000	466	1.58
			CO	kmol/h	6035	6100	65	1.08
			CH_4	kmol/h	1435	1460	25	1.74
			C_2H_4	kmol/h	2179	2200	21	0.96
			C_2H_6	kmol/h	351	360	9	2.56
			C_3H_6	kmol/h	1649	1680	31	1.88
			C_3H_8	kmol/h	237	240	3	1.27
			C_4H_8	kmol/h	821	830	9	1.1
			C_4H_{10}	kmol/h	150	155	5	3.33
			C_5^+	kmol/h	183	185	2	1.09

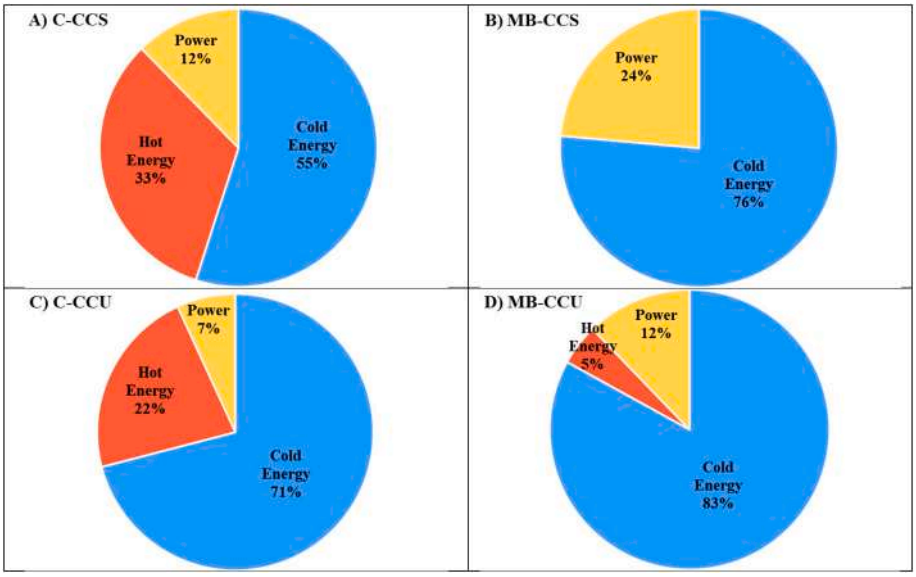

Fig. 10. Comparative Breakdown of Total Energy Demand by Energy Type (Power, Hot, and Cold) Across Conventional and Membrane-Based CCS and CCU Configurations.

intensification in fewer units, particularly in membrane configurations, complements the transition from thermal to mechanical energy discussed in Fig. 10, with clear implications for process optimization and utility integration.

3.3. Comparative KPI Analysis of CCS and CCU Configurations

Fig. 12 presents a comparative assessment of key performance indicators (KPIs) normalized per 1 MW of net electricity for the C-CCS, MB-CCS, C-CCU, and MB-CCU configurations. In the CCS schemes, the captured CO_2 is directed to storage and no fuel is produced; consequently, their chemical efficiency is zero. In contrast, the CCU configurations convert the separated CO_2 into valuable products, resulting in positive chemical efficiencies. Among them, C-CCU exhibits the highest value (0.34), marginally exceeding MB-CCU (0.31).

Although the absolute biogas feed rate remains constant across all scenarios, the BioGas Demand (BGD) index is higher in membrane-based systems (2.11 vs. 1.97 in CCS and 1.80 vs. 1.42 in CCU). This difference primarily reflects the lower net electricity output of the membrane configurations due to additional internal power consumption (e.g., compressors and auxiliary equipment), rather than an increase in actual biogas throughput.

Utility requirements reveal substantial structural differences between capture-only and utilization pathways. The CCU configurations

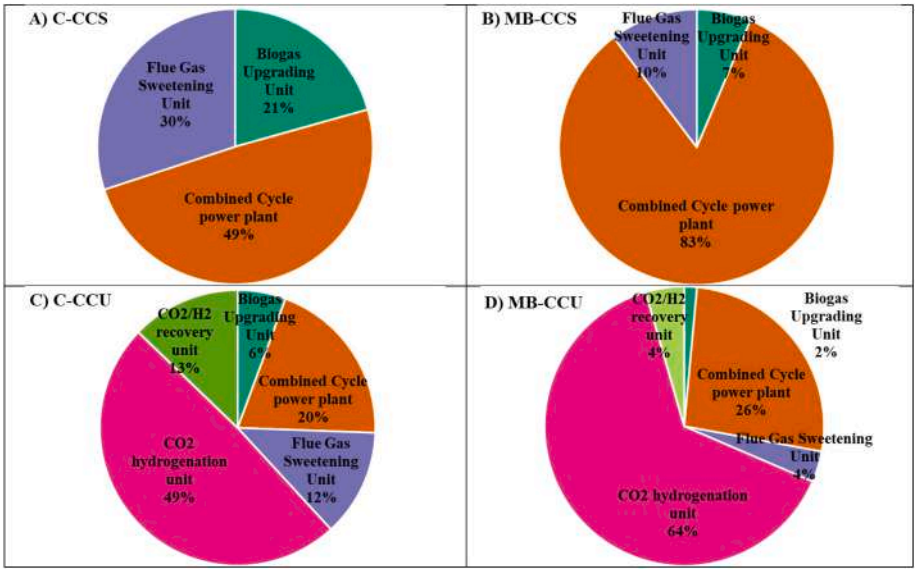

Fig. 11. Comparative Unit-Wise Distribution of Total Energy Consumption in Conventional and Membrane-Based CCS and CCU Systems.

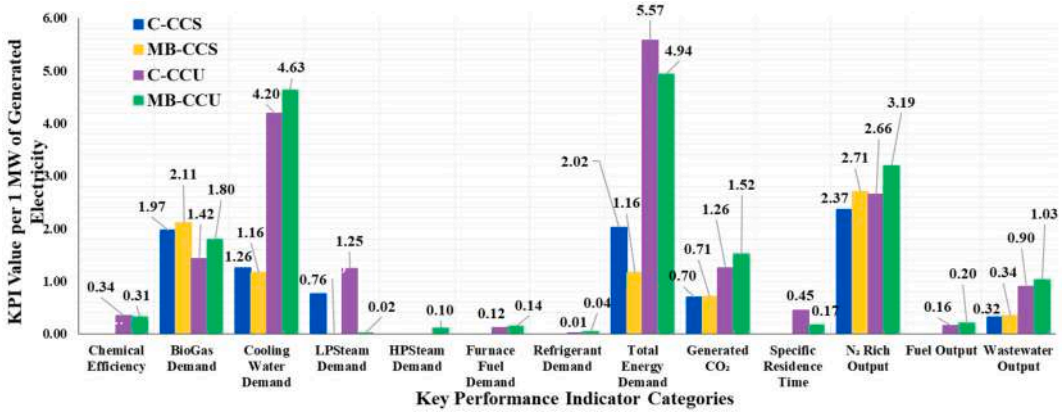

Fig. 12. KPI comparison per 1 MW of net power for C-CCS, MB-CCS, C-CCU, and MB-CCU.

require significantly higher cooling water demand (4.20–4.63), approximately three to four times that of CCS (1.16–1.26), owing to synthesis reactions and downstream condensation processes. Importantly, membrane integration leads to a pronounced reduction in LP steam demand. MB-CCS eliminates LP steam consumption entirely (0.00 vs. 0.76 in C-CCS), while MB-CCU reduces it drastically (0.02 vs. 1.25 in C-CCU). This reduction is primarily due to the use of membrane based separation units for biogas upgrading and for post combustion CO_2 removal. In contrast, conventional amine absorption systems require a significant amount of LP steam because solvent regeneration in the stripper reboiler is an energy intensive step. Since membrane separation relies only on pressure driven transport and does not involve any solvent regeneration, the membrane based configuration requires no LP steam.

Consequently, the total energy demand of MB-CCS decreases to 1.16, corresponding to a 42.6% reduction compared with conventional CCS (2.02). Likewise, MB-CCU achieves a 12.8% lower total energy demand than C-CCU (4.94 vs. 5.57), mainly driven by the substantial decrease in thermal utility requirements.

Regarding carbon management, it is important to distinguish between storage and utilization pathways. In CCS configurations, the separated CO_2 is permanently stored, whereas in CCU configurations it is internally consumed and transformed into products. The "Generated CO_2" indicator therefore represents the quantity of CO_2 separated from biogas upgrading and flue-gas sweetening per unit of net electricity. MB-CCS exhibits nearly identical values to C-CCS (0.71 vs. 0.70 t/MWh), indicating comparable capture performance. In the CCU configurations, MB-CCU shows a higher normalized value (1.52 vs. 1.26 t/MWh), which is largely attributed to the lower net power output of the membrane case rather than a proportionally higher absolute CO_2 generation.

Membrane integration further improves the recovery of the N_2-rich stream in both operational modes, increasing the normalized output by 14.3% in CCS (2.71 vs. 2.37 t/MWh) and 19.9% in CCU (3.19 vs. 2.66 t/MWh). In addition, MB-CCU delivers a 25% higher fuel output (0.20 vs. 0.16 t/MWh). Notably, the specific residence time (SRT) decreases from 0.45 to 0.17 min/MW in the membrane-based CCU case, corresponding to an approximately 62% reduction. Under comparable hydrodynamic and operating conditions, residence time scales with reactor holdup volume; therefore, this reduction implies that the required reactor volume per unit of net power can be reduced by a similar order of magnitude. Such volumetric downsizing directly translates into meaningful capital cost savings by lowering reactor size, associated internals, and auxiliary equipment requirements, thereby strengthening the techno-economic attractiveness of the membrane-integrated CCU pathway.

Overall, membrane integration demonstrates tangible structural advantages in both CCS and CCU pathways. In MB-CCS, the substantial reduction in thermal utility demand—particularly the elimination of low-pressure steam—translates into a markedly lower total energy requirement without compromising carbon capture performance. In

MB-CCU, the pronounced decrease in specific residence time reflects enhanced mass transfer and reaction effectiveness, enabling a significantly smaller reactor volume per unit of power and, consequently, meaningful reductions in capital expenditure. The observed improvements in fuel output and recovery of the N_2-rich stream further indicate strengthened separation efficiency and process integration. Although membrane systems impose a higher internal electricity load, this represents a shift in energy form rather than a fundamental penalty, aligning the process more closely with electrified and renewable-based energy infrastructures.

3.4. Comparative Economic Analysis of all proposed schemes

Fig. 13 compares the cost breakdowns of the various proposed schemes. As shown, replacing the conventional MEA absorber column with a membrane train reduces the overall capital requirement of the stand-alone CCS scheme by approximately 12%. Although the additional membrane modules increase the vessel and membrane costs from 0.6 MUSD to 1.6 MUSD, the compact configuration enables smaller compressors, pumps, and heat exchangers. As a result, the total equipment cost remains almost unchanged, increasing only slightly from 8.2 to 8.4 MUSD. The main savings arise from site-related expenses. Eliminating the 30 m column, deep foundations, and extensive piping reduces installation costs by 18%, from 17.2 to 14.1 MUSD, while offsite facilities decrease by 11%, from 5.4 to 4.8 MUSD. These reductions are reflected in the overall capital structure, with total fixed capital decreasing from 32.6 to 28.7 MUSD and working capital from 8.2 to 7.2 MUSD. Consequently, total capital cost declines from 40.8 to 35.9 MUSD, corresponding to an overall reduction of about 12%.

The economic advantage becomes more pronounced when the capture unit is integrated with a CO_2 valorization loop. Replacing the large slurry-phase reactor or adsorption section with a compact membrane reactor reduces reactor and adsorption costs from 11.9 to 5.8 MUSD. Together with simplified heat-exchange requirements, this reduces the total equipment cost by about 16%, from 25.9 to 21.7 MUSD. The smaller process footprint further lowers installation costs by 28%, from 56.0 to 40.5 MUSD, and reduces offsite infrastructure costs by 24%, from 17.5 to 13.3 MUSD. As a result, total fixed capital decreases from 104.9 to 79.5 MUSD and working capital from 26.2 to 19.9 MUSD. Overall capital expenditure is reduced from 131.1 to 99.4 MUSD, representing a 24% saving. In both CCS and CCU configurations, the primary economic benefit of membrane integration stems from reduced installation intensity rather than significant changes in base equipment pricing. A detailed comparative breakdown of major equipment cost components and unit-wise distribution for all four configurations (C-CCS, MB-CCS, C-CCU, and MB-CCU) is provided in the Supplementary Information (Figs. S6 and S7). Fig. 14 presents a unit-wise breakdown of CAPEX for conventional, MB-CCS, and CCU configurations. In the C-CCS case, the

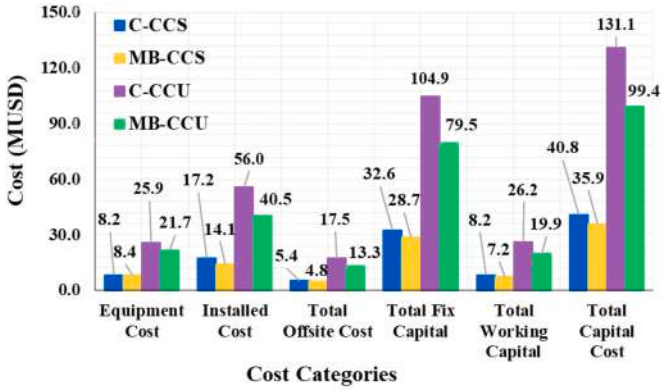

Fig. 13. Capital-Cost Breakdown Across Conventional and Membrane-Based CCS and CCU Configurations.

combined cycle power plant represents 52% of CAPEX, while the flue gas sweetening unit and the biogas upgrading unit contribute 29% and 19%, respectively. In the MB-CCS configuration, the combined-cycle power plant share rises to 58%, while the flue gas sweetening unit share falls to 27% and the biogas upgrading unit share to 15%. This shift reflects the redistribution of capital across units associated with the membrane-based layout, while the power island remains the dominant contributor.

In the C-CCU configuration, the CO_2 hydrogenation unit accounts for 41% of capital costs, followed by the CO_2/H_2 recovery unit at 20%, the combined cycle power plant at 22%, the flue gas sweetening unit at 11%, and the biogas upgrading unit at 6%. Upon integration of membranes, the CCU layout shows the hydrogenation unit remaining at 41% of expenditure, with the recovery unit at 12%, the flue gas sweetening unit at 13%, the combined cycle plant at 29%, and the biogas upgrading unit at 5%. The pronounced dominance of the hydrogenation step in both cases underscores its role as the principal driver of capital requirements in CCU systems.

Looking at the results in terms of operating expenditure (OPEX) across all four CCS and CCU configurations (Fig. 15), in the C-CCS system, the combined cycle power plant accounts for the largest share of OPEX (47%), followed by the flue gas sweetening unit (29%) and the biogas upgrading unit (24%). This distribution reflects the substantial utility and maintenance costs associated with steam regeneration and power generation. In contrast, in the MB-CCS configuration, the CCPP dominates the OPEX profile, accounting for 75%, while the sweetening and upgrading units contribute 16% and 9%, respectively. This shift aligns with the transition toward compression-driven processes, which elevate electricity-related operational costs.

For C-CCU, the cost distribution becomes more diversified due to the inclusion of downstream synthesis steps. The CO_2 hydrogenation unit emerges as the primary cost driver, accounting for 51% of total OPEX, followed by the CCPP (22%) and the CO_2/H_2 recovery unit (18%). The MB-CCU configuration shows a similar trend, with the hydrogenation unit maintaining a dominant share (49%) and the CCPP and recovery units contributing 25% and 11%, respectively. The biogas upgrading and sweetening units consistently represent minor cost components in all CCU cases. Overall, these findings highlight the economic burden of fuel synthesis and power generation, underscoring the need to optimize costs in high-energy units when shifting from conventional to membrane-based systems and from capture-only to utilization scenarios.

Table 11 compares the key financial performance indicators for the four configurations. Membrane integration significantly enhances economic viability across both CCS and CCU applications. In CCS systems, the membrane-based pathway increases NPV from 72 to 86 MUSD, raises IRR from 16.8% to 20.3%, and shortens the payback period from 8.9 to 6.9 years. In parallel, LCOE decreases from 101 to 79 USD/MWh, reflecting improved cost efficiency in electricity generation. However, LCNC increases from 207 to 254 USD/t CO_2, indicating a higher cost per ton of avoided CO_2 under the membrane-based configuration. Net profit also rises modestly from 6.9 to 7.4 MUSD/year, confirming a moderate improvement in overall project profitability.

In CCU configurations, membrane integration yields greater financial gains. NPV increases from 135 to 169 MUSD, IRR rises from 12.6% to 15.6%, and the payback period decreases from 12.6 to 10.2 years. Net profit improves slightly from 25.0 to 25.7 MUSD/year. In contrast to the CCS case, LCNC decreases from 161 to 138 USD/t CO_2, indicating improved carbon-cost performance for utilization pathways. A substantial reduction in LCOE is also observed, from 98 to 42 USD/MWh, highlighting the stronger economic leverage of membrane integration when coupled with CO_2 utilization. Overall, the results suggest that membrane-based configurations enhance financial attractiveness in both capture-only and utilization scenarios, with particularly notable benefits in CCU systems due to improved revenue generation and lower carbon cost intensity.

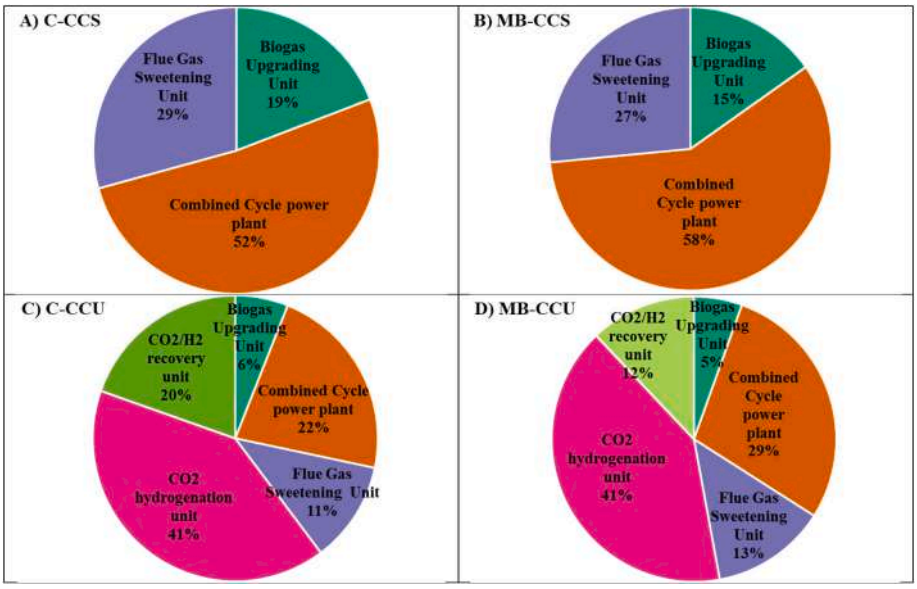

Fig. 14. Comparative Unit-Wise Distribution of CAPEX in Conventional and Membrane-Based CCS and CCU Configurations.

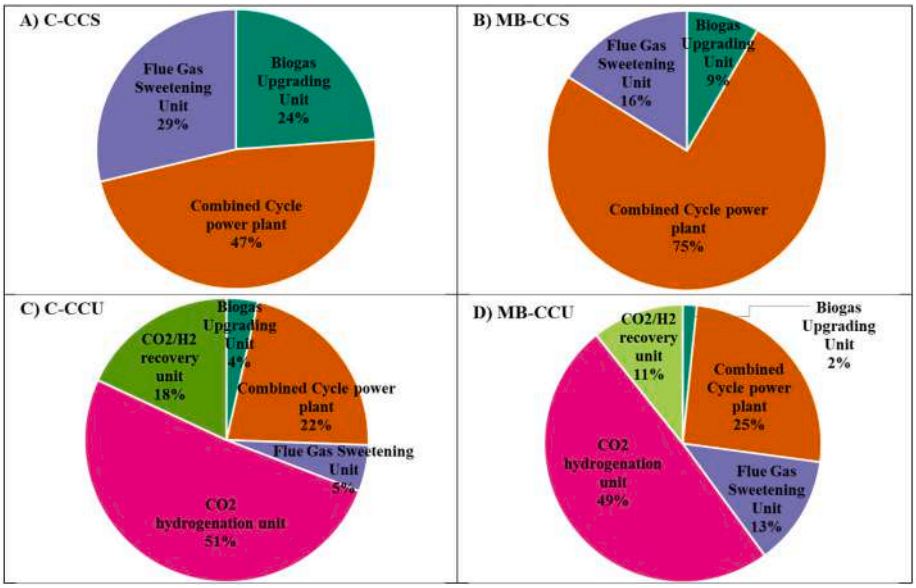

Fig. 15. Comparative Unit-Wise Distribution of OPEX in Conventional and Membrane-Based CCS and CCU Configurations.

Table 11
Comparison of Key Financial Performance Metrics for Conventional vs. Membrane-Based CCS and CCU Configurations.

Parameter	C-CCS (MUSD)	MB-CCS (MUSD)	C-CCU (MUSD)	MB-CCU (MUSD)
Total NPV (MUSD)	72	86	135	169
IRR,%	16.8	20.3	12.6	15.6
PBP, Year	8.9	6.9	12.6	10.2
LCOE (USD/MWh)	101	79	98	42
LCNC (USD/t CO_2)	207	254	161	138
Net Profit (MUSD/year)	6.9	7.4	25.0	25.7

3.5. Sensitivity analysis

Fig. 16 presents a comprehensive parametric sensitivity analysis of the LCOE and PBP for conventional and membrane-based CCS and CCU configurations. The figure evaluates the response of financial indicators to variations in major economic parameters such as feedstock cost, utility prices, and policy-related charges, thereby assessing the financial resilience of each configuration under different market scenarios.

Biogas cost exhibits a pronounced impact on system economics. A 300% increase in its price results in a substantial rise in the LCOE across all configurations. For example, in the MB-CCU case, LCOE increases from 49 to 148 USD/MWh, while the PBP extends from 10.3 to 13.4 years. In MB-CCS, LCOE rises from 54 to 153 USD/MWh, and PBP increases from 6.2 to 10.7 years. This confirms that all pathways remain sensitive to feedstock pricing, although CCS configurations maintain shorter payback periods than CCU cases across the range.

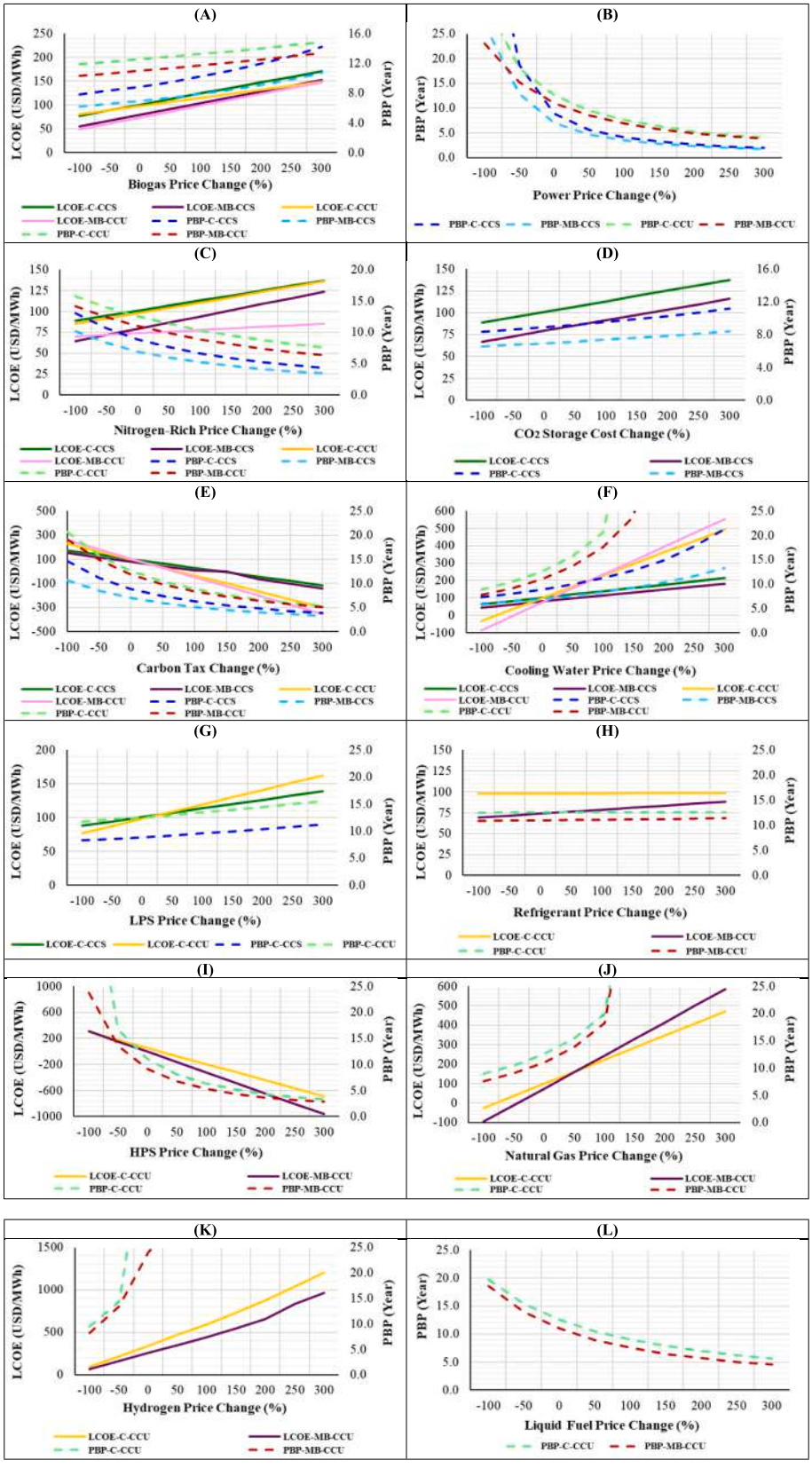

Fig. 16. Sensitivity Analysis of LCOE and Payback Period to Key Economic Inputs across Conventional and MB-CCS and MB-CCU Pathways.

The electricity price primarily affects payback rather than LCOE in the presented tables. As electricity prices increase from −100% to +300%, the PBP of MB-CCU decreases from 23.0 to 3.8 years, while that of C-CCU decreases from 32.0 to 4.0 years. In the zero-price case, CCS configurations do not achieve capital recovery within a practical project lifetime. This demonstrates the strong dependence of project viability on power market conditions and electricity incentives.

Nitrogen-rich utility shows a dual and somewhat counterintuitive effect. As the nitrogen-rich utility price increases from −100% to +300%, LCOE rises, for example, in the MB-CCU case from 70 to 85 USD/MWh, while PBP simultaneously improves from 14.2 to 6.3 years. This behavior arises because higher nitrogen-rich utility revenue strengthens project cash flow and shortens the payback period, but it also affects tax calculations and cost allocation within the LCOE framework. Consequently, although LCOE increases, overall financial performance improves, as evidenced by a shorter payback period, driven by enhanced revenue streams.

HPS cost affects only the CCU configurations, as this utility is associated with the hydrogenation and syngas-related sections and is absent from CCS pathways. CCU systems show strong sensitivity to variations in HPS pricing. As HPS cost changes from −100% to +300%, LCOE in the MB-CCU case decreases from 313 to −964 USD/MWh, while the payback period improves from 23.8 years to 2.8 years. A similar pattern is observed in C-CCU, where LCOE decreases from 307 to −696 USD/MWh, and the system shifts from failing to achieve capital recovery at low HPS values to a 3.3-year payback period at high HPS values. The negative LCOE values indicate that the revenue associated with HPS becomes sufficiently large to outweigh the annualized production costs, effectively transforming electricity into a secondary revenue stream. In this situation, overall project profitability is primarily driven by coproduct value rather than power generation alone.

CO_2 storage cost affects only CCS pathways. As storage cost increases from −100% to +300%, LCOE in C-CCS rises from 89 to 137 USD/MWh, and PBP increases from 8.3 to 11.1 years. MB-CCS shows a similar trend, with LCOE rising from 67 to 116 USD/MWh and PBP from 6.6 to 8.4 years. CCU configurations remain unaffected.

Carbon tax exerts a strong influence across all systems. As the carbon tax increases from −100% to +300%, LCOE in MB-CCU decreases from 257 to −353 USD/MWh, and PBP improves from 19.1 to 5.1 years. CCS pathways also benefit, with C-CCS PBP decreasing from 14.6 to 3.9 years. Negative LCOE values at high carbon pricing reflect the dominance of carbon credit revenue over annualized electricity production costs.

Cooling water cost moderately affects CCS but strongly impacts CCU. In MB-CCU, LCOE increases from −86 to 553 USD/MWh, and PBP increases from 7.8 years to a point where the system does not achieve capital recovery at high cooling cost levels. CCS pathways remain comparatively stable, with PBP ranging from 7.3 to 21.3 years in C-CCS and 5.9 to 13.3 years in MB-CCS.

Low-pressure steam shows a limited impact. In C-CCS, LCOE increases from 88 to 139 USD/MWh, and PBP rises from 8.3 to 11.3 years. In C-CCU, LCOE increases from 76 to 162 USD/MWh, and PBP from 11.8 to 15.6 years, confirming a secondary influence relative to major energy carriers. Refrigerant cost affects only CCU configurations. As refrigerant price increases from −100% to +300%, LCOE in MB-CCU increases from 69 to 89 USD/MWh, while PBP changes only slightly from 10.9 to 11.4 years, indicating a comparatively minor financial impact. The cost of natural gas significantly affects CCU systems that rely on syngas production. As natural gas prices increase from −100% to +300%, the LCOE of the MB-CCU increases from −96 to 584 USD/MWh; above +150%, the system does not achieve capital recovery. CCS configurations remain largely unaffected, confirming their lower exposure to natural gas price volatility.

Direct hydrogen purchase, rather than producing hydrogen internally from a syngas package, is the most critical economic risk in CCU systems. When hydrogen is externally supplied at market prices, the project becomes highly exposed to price volatility. As an alternative, this study considers the integration of an on-site syngas production package in which natural gas serves as the primary feedstock. In this configuration, hydrogen is generated internally through reforming, and the associated HPS produced during the process is recovered as a valuable by-product. Assuming an effective hydrogen production cost of approximately 1500 USD/t under this integrated setup, the sensitivity analysis demonstrates markedly improved economic stability compared to direct hydrogen purchase.

When hydrogen is purchased at prevailing market prices (around 3000 USD/t), CCU pathways rapidly lose economic viability, and capital recovery cannot be achieved within a practical project lifetime under moderate price increases.

In contrast, when hydrogen is produced internally via the syngas package and the steam by-product is valorized, both LCOE and PBP improve significantly, consistent with the HPS sensitivity results. The additional steam revenue strengthens cash flow and partially offsets fluctuations in natural gas prices.

These results clearly indicate that purchasing hydrogen at high market prices is not economically rational for CCU configurations. Sustainable operation requires either on-site hydrogen production through reforming or reliable access to structurally low-cost hydrogen sources. Without such integration, CCU economics remain highly vulnerable to hydrogen price volatility and struggle to deliver acceptable investment returns.

In summary, biogas, electricity, hydrogen, natural gas, and carbon pricing are the dominant economic drivers shaping both LCOE and payback. Utility parameters such as steam and refrigerant have secondary influence. Negative LCOE values arise when coproduct or policy revenues exceed annualized electricity production costs and should be interpreted as strong net profitability rather than negative physical generation cost.

Fig. 17 presents a sensitivity analysis of LCOE and PBP for MB-CCS and MB-CCU systems, highlighting the effects of membrane cost and lifetime. The base case assumes a CMS membrane lifetime of 3 years and a membrane cost as listed in Table 6. The cost of CMS membranes significantly affects both metrics. A 100% cost reduction lowers LCOE to 71 USD/MWh (CCS) and 63 USD/MWh (CCU), with PBPs decreasing to 5.8 and 10.1 years, respectively. Conversely, a 300% cost increase raises LCOE to 104 USD/MWh (CCS) and 106 USD/MWh (CCU), while PBPs increase to 11.4 and 13.9 years, respectively.

Increasing CMS lifetime from 1 to 9 years decreases LCOE from 97 to 71 USD/MWh for CCS and from 97 to 63 USD/MWh for CCU. Over the same range, PBP decreases from 7.6 to 6.7 years in CCS and from 11.7 to 10.7 years in CCU, indicating a moderate but consistent improvement in financial performance.

Silica membrane cost has a relatively modest influence on CCU economics, with LCOE ranging from 72 to 79 USD/MWh and PBP changing slightly from 10.8 to 11.5 years.

Extending silica membrane lifetime from 1 to 9 years reduces LCOE from 77 to 72 USD/MWh, while PBP remains nearly constant around 11.1 to 10.9 years, indicating limited sensitivity to this parameter. Reactor membrane cost has a stronger impact on CCU performance. As its cost varies from −100% to +300%, LCOE changes from 62 to 109 USD/MWh, and PBP increases from 10.0 to 14.1 years. Increasing reactor membrane lifetime from 1 to 9 years decreases LCOE from 106 to 59 USD/MWh, while PBP improves from 11.9 to 10.6 years, showing that durability improvements provide incremental but measurable economic benefits.

Overall, both membrane cost and membrane lifetime play important roles in the economic performance of membrane based CCS and CCU systems. The sensitivity analysis shows that increasing membrane lifetime improves the economic indicators, leading to lower LCOE and shorter PBP. However, the results also indicate that the system economics are more sensitive to membrane cost than to membrane lifetime, since membrane price directly affects the initial capital investment,

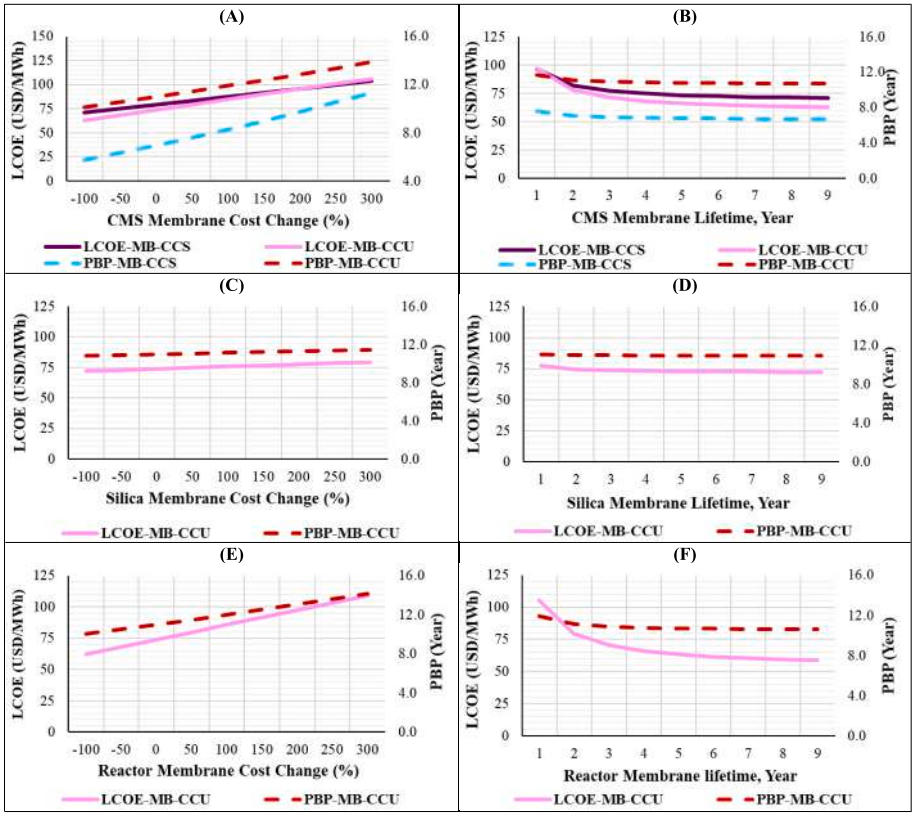

Fig. 17. Sensitivity Analysis of LCOE and Payback Period to Membrane Cost and Lifetime Parameters in MB-CCS and MB-CCU Configurations.

whereas replacement costs occur later during plant operation and are discounted in the economic evaluation. Therefore, reducing membrane cost while simultaneously improving membrane durability, particularly for CMS and reactor membranes, remains a key factor for enhancing the techno economic feasibility of these systems.

4. Conclusion and future trends

This study presents a unified techno-economic assessment of conventional and membrane-enabled CCS and CCU integrated into small-scale biogas-fired combined-cycle power plants. For the first time, a fully membrane-based post-combustion CO_2 capture unit for CCS and a membrane reactor–assisted CCU configuration are evaluated side by side within a consistent Aspen HYSYS framework under identical system boundaries. All subsystems were simulated and validated against reference data (±5%). Membrane integration improved energy performance by eliminating hot-utility demand and reducing specific energy consumption by 43% in CCS. At comparable CO_2 conversion, the membrane reactor achieved higher hydrocarbon selectivity at shorter residence times and smaller reactor volumes than the conventional reactor, demonstrating clear process-intensification benefits. Specifically, the specific residence time decreased by approximately 62%, indicating a comparable reduction in required reactor volume per unit power and associated capital expenditure. Capital expenditure decreased by 12% for CCS and up to 24% for CCU. For CCS, NPV increased from 72 to 86 MUSD, IRR from 16.8% to 20.3%, and payback shortened from 8.9 to 6.9 years. For CCU, NPV rose from 135 to 169 MUSD, IRR from 12.6% to 15.6%, and payback decreased from 12.6 to 10.2 years. Although membrane reactor-assisted CCU required higher utilities, it increased value-added fuel production by 31.3%, highlighting the trade-off between intensified conversion and energy demand. Sensitivity analysis identified membrane cost, lifetime, and utility prices as the main LCOE drivers. In syngas-based CCU, a 300% rise in natural gas prices increased LCOE from −96 to 584 USD/MWh, while hydrogen prices above 3000 USD/t rendered several pathways unviable. Overall, membrane-enabled CCS and CCU offer substantial energy and economic benefits for decentralised biogas-fired power systems, provided membrane performance and hydrogen costs are optimised.

CRediT authorship contribution statement

Mostafa Jafari: Writing – original draft, Investigation, Formal analysis, Data curation, Conceptualization. **Kamran Ghasemzadeh:** Writing – review & editing, Writing – original draft, Supervision, Methodology, Investigation, Conceptualization. **Maria-Chiara Ferrari:** Writing – review & editing, Supervision, Investigation. **Adele Brunetti:** Writing – review & editing, Supervision, Funding acquisition. **Simona Liguori:** Writing – review & editing, Supervision. **Rashid Jamshidi:** Writing – review & editing, Writing – original draft, Supervision.

Declaration of competing interest

The authors declare that they have no known competing financial interests or personal relationships that could have appeared to influence the work reported in this paper.

Acknowledgements

Kamran Ghasemzadeh and Maria Chiara Ferrari gratefully acknowledge funding from the European Union's Horizon Europe research and innovation programme under Grant Agreement No. 101115488 (project DAM4CO2), and from UK Research and Innovation (UKRI) under the UK Government's Horizon Europe funding guarantee, Grant No. 10083164. Adele Brunetti gratefully acknowledges funding from the European Union – NextGeneration EU from the Italian Ministry of Environment and Energy Security POR H2 AdP MMES/ENEA with

involvement of CNR and RSE, PNRR - Mission 2, Component 2, Investment 3.5 “Ricerca e sviluppo sull'idrogeno”, CUP: B93C22000630006.

Appendix A. Supplementary data

Supplementary data to this article can be found online at https://doi.org/10.1016/j.fuproc.2026.108449.

Data availability

Data will be made available on request.

References

[1] A. Nsabiyeze, R. Ma, J. Li, H. Luo, Q. Zhao, J. Tomka, M. Zhang, Tackling climate change in agriculture: a global evaluation of the effectiveness of carbon emission reduction policies, J. Clean. Prod. 468 (2024) 142973.

[2] IEA, 20 Years of Carbon Capture and Storage - Accelerating Future Deployment, International Energy Agency (IEA), 2016. https://www.iea.org/reports/20-years-of-carbon-capture-and-storage (accessed March 15, 2025).

[3] A. Al-Mamoori, A. Krishnamurthy, A.A. Rownaghi, F. Rezaei, Carbon capture and utilization update, Energ. Technol. 5 (2017) 834–849.

[4] R.M. Cuéllar-Franca, A. Azapagic, Carbon capture, storage and utilisation technologies: a critical analysis and comparison of their life cycle environmental impacts, J. CO_2 Util. 9 (2015) 82–102.

[5] A. Izadpanahi, M.J. Blunt, N. Kumar, M. Ali, C.C.G. Tassinari, M.A. Sampaio, A review of carbon storage in saline aquifers: Mechanisms, prerequisites, and key considerations, Fuel 369 (2024) 131744.

[6] E.S. Rubin, J.E. Davison, H.J. Herzog, The cost of CO2 capture and storage, Int. J. Greenh. Gas Con. 40 (2015) 378–400.

[7] R. Kumar, C. Zhang, A.K. Itta, W.J. Koros, Highly permeable carbon molecular sieve membranes for efficient CO2/N2 separation at ambient and subambient temperatures, J. Membr. Sci. 583 (2019) 9–15.

[8] M. Cao, L. Zhao, D. Xu, R. Ciora, P.K.T. Liu, V.I. Manousiouthakis, T.T. Tsotsis, A carbon molecular sieve membrane-based reactive separation process for pre-combustion CO2 capture, J. Membr. Sci. 605 (2020) 118028.

[9] M. Joglekar, A.K. Itta, R. Kumar, G.B. Wenz, J. Mayne, P.J. Williams, W.J. Koros, Carbon molecular sieve membranes for CO2/N2 separations: evaluating subambient temperature performance, J. Membr. Sci. 569 (2019) 1–6.

[10] M. Hou, L. Li, R. Xu, Y. Lu, J. Song, Z. Jiang, T. Wang, X. Jian, Precursor-chemistry engineering toward ultrapermeable carbon molecular sieve membrane for CO2 capture, J. Energy Chem. 102 (2025) 421–430.

[11] M. Elwardany, A.M. Nassib, H.A. Mohamed, Analyzing global research trends in combined cycle power plants: a bibliometric study, Energy Nexus 13 (2024) 100265.

[12] M. Zoghi, N. Hosseinzadeh, S. Gharaie, A. Zare, Waste heat recovery of a combined Brayton and inverse Brayton cycle for gas turbine based multi-generation hydrogen and freshwater purposes: 4E comparison with a simple coupled Brayton and inverse Brayton cycle, Therm. Sci. Eng. Prog 53 (2024) 102718.

[13] M. Van Der Spek, D. Bonalumi, G. Manzolini, A. Ramirez, A. Faaij, Techno-economic comparison of combined cycle gas turbines with advanced membrane configuration and monoethanolamine solvent at part load conditions, Energy Fuel 32 (2018) 625–645.

[14] J. Asadi, P. Kazempoor, Techno-economic analysis of membrane-based processes for flexible CO2 capturing from power plants, Energy Convers. Manag. 246 (2021) 114633.

[15] E. Akrami, S. Khalilarya, M.V. Rocco, Techno-economic evaluation of a novel bio-energy system integrated with carbon capture and utilization technology in greenhouses, J. Taiwan Inst. Chem. Eng. 148 (2023) 104729.

[16] E. Hanson, C. Nwakile, V.O. Hammed, Carbon capture, utilization, and storage (CCUS) technologies: evaluating the effectiveness of advanced CCUS solutions for reducing CO2 emissions, Results Surf. Interfaces 18 (2024) 100381.

[17] S. Nagireddi, J.R. Agarwal, D. Vedapuri, Carbon dioxide capture, utilization, and sequestration: current status, challenges, and future prospects for global decarbonization, AC Eng. Au. 4 (2023) 22–48.

[18] W. Yaïci, E. Entchev, M. Longo, Recent advances in Small-Scale carbon capture systems for Micro-combined heat and power applications, Energies (Basel) 15 (2022) 2938.

[19] G.G. Esquivel-Patiño, F. Nápoles-Rivera, A. Jiménez-Gutiérrez, Implementation of carbon utilization technologies and thermodynamic organic rankine cycles in biogas combined cycle power plants, Thermo 5 (2025) 43.

[20] K. Ghasemzadeh, M. Jafari, A. Sari, A.A. Babalou, Performance investigation of membrane process in natural gas sweeting by membrane process: Modeling study, Chem. Prod. Process. Model. 11 (2016) 23–27.

[21] M. Jafari, M.S. Deljoo, A. Vatani, Simulation and economic evaluation of polygeneration system for coproduction of power, steam, CH3OH, h2, and CO2 from flare gas, Iran. J. Oil Gas Sci. Technol. 9 (2020) 93–114, https://doi.org/10.22050/ijogst.2020.227023.1547.

[22] M. Jafari, M.-H. Sarrafzadeh, K. Ghasemzadeh, Simulation and economic evaluation of heat and power generation from flare gases in a combined cycle power plant, Energy Equip. Syst. 8 (2020) 307–322.

[23] M. Jafari, K. Ghasemzadeh, T. Yusefi Amiri, A. Basile, Comparative study of membrane and absorption processes performance and their economic evaluation for CO2 capturing from flue gas, Gas Process. J. 7 (2019) 37–52.

[24] M. Jafari, M. Nezhadfard, A. Khalili-Garakani, Simulation and economic analysis of combined desalinated water and power generation from associated gases of cheshmeh khosh, Iran. J. Oil Gas Sci. Technol. 10 (2021) 1–14.

[25] E. Smith, J. Morris, H. Kheshgi, G. Teletzke, H. Herzog, S. Paltsev, The cost of CO2 transport and storage in global integrated assessment modeling, Int. J. Greenh. Gas Con. 109 (2021) 103367.

[26] A. Calbry-Muzyka, H. Madi, F. Rüsch-Pfund, M. Gandiglio, S. Biollaz, Biogas composition from agricultural sources and organic fraction of municipal solid waste, Renew. Energy 181 (2022) 1000–1007.

[27] A. Rahimalimamaghani, R. Ramezani, D.A.P. Tanaka, F. Gallucci, Carbon molecular sieve membranes for selective CO2/CH4 and CO2/N2 separation: Experimental study, optimal process design, and economic analysis, Ind. Eng. Chem. Res. 62 (2023) 19116–19132.

[28] S. Najari, G. Gróf, S. Saeidi, F. Gallucci, Modeling and optimization of hydrogenation of CO2: Estimation of kinetic parameters via artificial bee colony (ABC) and differential evolution (DE) algorithms, Int. J. Hydrog. Energy 44 (2019) 4630–4649.

[29] T.N. Do, J. Kim, Green C2-C4 hydrocarbon production through direct CO2 hydrogenation with renewable hydrogen: Process development and techno-economic analysis, Energy Convers. Manag. 214 (2020) 112866.

[30] O. Eterigho-Ikelegbe, S.O. Bada, M.O. Daramola, Preparation and evaluation of nanocomposite sodalite/α-Al2O3 tubular membranes for H2/CO2 separation, Membranes (Basel). 10 (2020) 312.

[31] S. Khajavi, J.C. Jansen, F. Kapteijn, Application of a sodalite membrane reactor in esterification—Coupling reaction and separation, Catal. Today 156 (2010) 132–139, https://doi.org/10.1016/j.cattod.2010.02.042.

[32] K. Ghasemzadeh, A. Aghaeinejad-Meybodi, M.J. Vaezi, A. Gholizadeh, M.A. Abdi, A.A. Babaluo, M. Haghighi, A. Basile, Hydrogen production via silica membrane reactor during the methanol steam reforming process: Experimental study, RSC Adv. 5 (2015) 95823–95832.

[33] M. Jafari, V. Spallina, K. Ghasemzadeh, Techno-economic assessment of flare gas valorisation during membrane-based GTL process by net-zero strategy, Energy Convers. Manag. 315 (2024) 118796.

[34] L.E. Øi, A. Haukås, S. Aromada, N. Eldrup, Automated cost optimization of CO2 capture using aspen HYSYS, SIMS (2022) 293–300.

[35] S. Leptinsky, M. Turner, M. Oaks, D. Quinn, J. Gummoe, S. Homsy, T. Teel, P. Cvetic, N. Kuehn, M. Woods, Examination of Factors Affecting the cost and Performance of a Natural Gas combined Cycle equipped with Carbon Dioxide Capture, National Energy Technology Laboratory (NETL), Pittsburgh, PA, Morgantown, WV, 2025.

[36] G. Di Marcoberardino, D. Vitali, F. Spinelli, M. Binotti, G. Manzolini, Green hydrogen production from raw biogas: a techno-economic investigation of conventional processes using pressure swing adsorption unit, Processes 6 (2018) 19.

[37] A. Palizdar, A. Vatani, Design and analysis of a novel self-refrigerated natural gas liquefaction system integrated with helium recovery and CO2 liquefaction processes, J. Clean. Prod. 423 (2023) 138600, https://doi.org/10.1016/j.jclepro.2023.138600.

[38] G. Towler, R. Sinnott, Chemical Engineering Design: Principles, Practice and Economics of Plant and Process Design, Butterworth-Heinemann, 2021.

[39] IHS Markit, Advanced Technology Natural Gas Combined Cycle, Process Economics Program (PEP), 2013.

[40] A. Naquash, M.A. Qyyum, Y.D. Chaniago, A. Riaz, F. Yehia, H. Lim, M. Lee, Separation and purification of syngas-derived hydrogen: a comparative evaluation of membrane-and cryogenic-assisted approaches, Chemosphere 313 (2023) 137420.

[41] S. Roussanaly, E.S. Rubin, M. van der Spek, G. Booras, N. Berghout, T. Fout, M. Garcia, S. Gardarsdottir, V.N. Kuncheekanna, M. Matuszewski, S. McCoy, J. Morgan, S. Mohd Nazir, A. Ramirez, Towards Improved Guidelines for Cost Evaluation of Carbon Capture and Storage, Cheltenham, United Kingdom. https://ieaghg.org/publications/technical-reports, 2021.

[42] R. Hou, C. Fong, B.D. Freeman, M.R. Hill, Z. Xie, Current status and advances in membrane technology for carbon capture, Sep. Purif. Technol. 300 (2022) 121863.

[43] S. Richard, A.R. Santos, F. Gallucci, PEM gensets using membrane reactors technologies: an economic comparison among different e-fuels, Int. J. Hydrog. Energy 50 (2024) 433–457.

[44] N.L. Mohd Jailani, C.C. Phing, C.H. Tan, J. MILANO, G. Alkawsi, C.W. Lim, T. Sieh Kiong, Sustainable integration of wind and grid resources for electric vehicles charging in low wind speed region: a Techno-Economic assessment, Energy Convers. Manag: X 27 (2025) 101118.

[45] European Commission, Spring 2024 Economic Forecast: A Gradual Expansion amid High Geopolitical Risks. https://economy-finance.ec.europa.eu/economic-forecast-and-surveys/economic-forecasts/spring-2024-economic-forecast-gradual-expansion-amid-high-geopolitical-risks_en?utm_source=chatgpt.com, 2024 (accessed May 28, 2025).

[46] H. Breunig, F. Rosner, S. Saqline, D. Papadias, E. Grant, K. Brooks, T. Autrey, R. Ahluwalia, J. King, S. Hammond, Achieving gigawatt-scale green hydrogen production and seasonal storage at industrial locations across the US, Nat. Commun. 15 (2024) 9049.

[47] T. Hos, M. Herskowitz, Techno-economic analysis of biogas conversion to liquid hydrocarbon fuels through production of lean-hydrogen syngas, AC Eng. Au. 2 (2022) 450–460.

[48] U.S. Energy information administration (EIA), natural gas weekly Update. https://www.eia.gov/naturalgas/weekly/?utm_source=chatgpt.com, 2025.
[49] S. Patnaik, K. kennedy, Why The US Should Establish a Carbon Price Either Through Reconciliation or Other Legislation, 2021.
[50] A. Sanchez, V. Sevilla-Güitrón, G. Magaña, L. Gutierrez, Parametric analysis of total costs and energy efficiency of 2G enzymatic ethanol production, Fuel 113 (2013) 165–179.
[51] IMARC Group, Nitrogen Prices, Trend & Forecast IMARC Group Nitrogen Pricing Report. https://www.imarcgroup.com/nitrogen-pricing-report?utm_source=chatgpt.com, 2025 (accessed May 26, 2025).
[52] Choose Energy, Electricity Rates by State | May 2025. https://www.chooseenergy.com/electricity-rates-by-state, 2025 (accessed May 26, 2025).
[53] R.S. Cavaignac, N.L. Ferreira, R. Guardani, Techno-economic and environmental process evaluation of biogas upgrading via amine scrubbing, Renew. Energy 171 (2021) 868–880.
[54] P.A. Argyris, J. Wong, A. Wright, L.M.C. Pereira, V. Spallina, Reducing the cost of low-carbon hydrogen production via emerging chemical looping process, Energy Convers. Manag. 277 (2023) 116581.